Bio-fabrication and experimental validation of an Mg – 25Ca – 5Zn alloy proposed for a porous metallic scaffold.

Luis Humberto Campos Becerra
Universidad Autonoma de Nuevo Leon https://orcid.org/0000-0001-5619-4164
Marco Antonio Loudovic Hernández Rodríguez
UANL: Universidad Autonoma de Nuevo Leon
Jonathan Puente de León
UANL: Universidad Autonoma de Nuevo Leon
Raúl Lesso Arroyo
Instituto Tecnológico de Celaya: Instituto Tecnologico de Celaya
Hugo Esquivel Solís
Centro de Investigación y Asistencia en Tecnología y Diseño del Estado de Jalisco: Centro de Investigacion y Asistencia en Tecnologia y Diseno del Estado de Jalisco
Eduardo Núñez Pérez
Universidad La Salle - Noroeste
Alejandro Torres Castro (alejandro.torrescs@uanl.edu.mx)
UANL: Universidad Autonoma de Nuevo Leon https://orcid.org/0000-0002-3034-2568

Research article

Keywords: Porous magnesium scaffold, Casting of Mg base alloys, Morphological characterization, Viability cell, Micro- indentation, Toxicity.

Posted Date: January 18th, 2021

DOI: https://doi.org/10.21203/rs.3.rs-141009/v1

Version of Record: A version of this preprint was published at Crystals on November 19th, 2021. See the published version at https://doi.org/10.3390/cryst11111416.

Abstract

Background The bio-fabrication of a porous scaffold from a selection procedure of elements taking into account the biological behavior, using Magnesium (Mg) alloyed with Calcium (Ca) and Zinc (Zn), it could work as a treatment for specific pathologies in trauma and oncology, on the one hand, in osteosynthesis, contributing to osseointegration and contributing to infection control through the release of drugs, additionally, another possible attribute of this alloy would be to be used as a complementary treatment for osteosarcoma, this is due to the basification produced by oxidative degradation. (Attack on cancer cells)(1)(2)(3)(4).

Methods The evaluation of cell viability of an alloy of Mg − 25 wt% Ca + 5 wt% Zn will strengthen current perspectives on the use of Mg in the clinical evaluation of various treatments in trauma and oncology. Considerations on the preparation of an alloy of Mg − 25 wt% Ca + 5 wt% Zn and its morphological characterization, will help to understand the applicability for the development of new surgical techniques and lead to a deeper investigation in the conception of alternative treatments. However, it is very important to bear in mind the mechanical effect of elements such as Ca and Zn, on the degradation of the alloy matrix, the best alternative to predict the biological - mechanical potential starts with the selection of the essential - nutritional elements (5)(6)(7) and its mechanical evaluation by micro-indentation due to the fragility of the matrix (8)(9).

Results Therefore, the morphological evaluation of the specimens of Mg − 25 wt% Ca + 5 wt% Zn will show the crystallinity of the alloy; these results together generate a contribution regarding the design of biomedical alloys for use in treatments for various medical specialties.

Conclusions The results indicated that cell viability is not affected, and there are no morphological changes in the cells.

1 Introduction

Currently the use of biomaterials in various applications such as orthognathic surgery have driven the development of techniques using allografts, autologous implants and demineralized bone matrix (DBM), However, according to the American Association of Tissue Banks (AATB), a problem is created due to deregulation because it is required to harvest bone from the patient and / or corpse, causing risks of infections, morbidity and situations outside the legal margin(10)(11)(12)(13)(14)(15). A base biomaterial Mg − 25 wt% Ca + 5 wt% Zn that can be used as a scaffold for the fractured bone to recover, avoiding tissue laceration and re-operation, can provide a higher healing rate without the risks associated with the primary procedure (16)(17)(18)(19). For applications where a scaffold is required as a complement to manage a fracture, the proposal of a porous scaffold made of MgCa-Zn has become an interesting proposal (20)(21)(19), because the FDA determined that the products contained within a human demineralized bone matrix (DBM), do not comply with the provisions of Sect. 361 of the public health service law, mainly because they are not sterilizing agents (22). Other options such as synthetic bone

graft extenders have properties similar to cadaver bone, however they do not contain the necessary products to stimulate bone regeneration (23)(24)(21). The release of Mg ions in vivo conducive an accumulation of the element around the fracture sites, favoring the formation of cortical bone (25)(26). Another option is to use the bone morphogenetic protein, BMP-2, which has been shown to induce osteogenesis through cellular alteration producing fibrous tissue. Several authors have proposed using elements such as Ca and Zn to improve the behavior of Mg in vivo, nutritional and essential elements for the body should be the first option in optimizing Mg for biomedical purposes(27)(28)(29)(9)(30)(31)(32)(33)(34)(35)(36). This article intends to contribute judgment to the ISO / TC 194 / WG5 committee, on the results of cell viability for MgCa-Zn alloys due to the acceptable levels shown under the ISO-10993 evaluation(37)(38). There are currently organizations that have results from technovigilance programs that show favorable results for manufacturing medical devices from these alloys (29)(39). Figure 1 shows the combination of a straight CMF plate (craniomaxillofacial) and a proposed Mg-based porous scaffold for the reconstruction and lengthening of the mandibular body.

Figure 1 Lengthening of the mandibular body.

Designing a biomedical MgCa-Zn alloy with a degradable matrix and zero toxicity poses challenges and opportunities, mechanical resistance is a factor that must be resolved.(40) However, toxicity is a fundamental aspect, these considerations must be taken into account in the design stages, furthermore, the mole fraction ratio of the elements and their solubility limits are important to understand the mechanisms of grain growth and second phase formation (41)(42)(43), the alloy must withstand the biomechanical loads of the body for pathologies where a BDM scaffold is required (44)(45). Senkov et al reported in their study that Ca, Mg and Zn provide the highest packing efficiency of the amorphous state(46). Taking care of the content of the percentages of elements in the formulation of an alloy and relating it to degradation will offer benefits on the toxicological impact of the alloy, which can be verified in in vitro experimentation on the cell viability of the alloy(47). For this reason, keeping in mind the daily intake limits for each element is essential to promote biocompatibility in this type of alloys.

In the smelting of non-ferrous alloys, oxidation should be avoided, it is advisable to melt in a reductive atmosphere using gases such as Argon, SF6 and / or Flux, in addition, using a vacuum will reduce porosity and generate grain refining(15)(48)(49)(50). The diffusion controlled oxidation process obeys the parabolic law(50)(51).

Micro-indentation techniques have allowed the analysis of data such as force-displacement from small volumes of material, from which the elastic modulus and hardness can be obtained, this application has allowed experimentation in trabecular, osteonal and lamellar bone, with this technique it is possible to explore the anisotropic elastic behavior of materials with lamellar formation, such as the case of the Mg – 25 wt% Ca + 5 wt% Zn alloy, where the MgCa2 phase has a lamellar-eutectic behavior, with these data it will be possible to understand more in depth about the theoretical development of fracture mechanisms (52)(53)(54)(55). A MgCa-Zn-based biomaterial that is used in the manufacture of a clinical implant will exhibit brittle behavior, which implies that failures occur due to exposure to cyclical loads due to fatigue,

However, due to Mg, this problem worsens, so identifying the morphology will serve as an initial effort to identify strategies that mitigate its degradation(33).

Mg as an element in an alloy contributes by inducing an anti-vibratory effect, for biomedical applications it is an excellent attribute due to its ability to absorb kinetic and potential energy, which may be a unique feature that helps counteract the shear loads that produce bone neo-formation (56).

Lui et al developed a histological evaluation on Mg-Zn and observed the formation of new trabeculae surrounded by osteoblasts and osteoclasts, consequently, they observed mature bone tissue and lamellar bone, as characteristics fundamental for the consolidation of bone regeneration(57)(58). Chang et al carried out a histological study in animals observing good tolerance of the organism to metal ions, showing from an early stage a biocompatible response(59). Sarkar et al report proliferation of osteocytes and mononuclear cells in the medullary cavity of a rabbit femur, indicating the beginning of an important healing process from Zn-doped MgP (60)(61).

2 Materials

An alloy of Mg – 25 wt% Ca + 5 wt% Zn of biological inspiration was formulated, which given the behavior of Mg will be degradable in vivo in approximately 150 days, considering the toxicological limits of Ca and Zn, which are considered nutritional and essential elements, these elements are normally found in the form of ions in the human body, while Zn frequently comes from the diet(30)(62)(63).

For the design of this alloy, it is proposed to use 69.18% Mg, 25.82% Ca and 4.99% Zn, considering a final weight for a device of 30 g, which corresponds to 20.75 g Mg, 7.74 g Ca and 1.49 g of Zn, if a linear degradation at 150 days is assumed and the permitted value in g / day for the human body is considered, these percentage and gram quantities for an alloy would not represent a toxicological risk for the organism. Using these percentages for the design of an alloy, the allowed value for these elements is not exceeded, Mg, Ca and Zn respectively show 0.14, 0.052 and 0.010 g / day, these values being well below the toxicological limit. See Table 1

This formulation is valid for class III implants or medical devices, weighing ≤ 30 g. Due to the risk associated with the use of Zn, the ideal weight proposed for the implant made from this alloy will be 30 g, raising the weight in g could cause an increase in the Zn content, this development proposes keeping the Zn in a lower percentage, the following criterion was used, not to exceed 60% of the toxicological limit of Zn, which leaves us a value of 0.010 g / day, it should be considered that the average nutritional diet of people can enrich the content of this element in the body and for this reason a low Zn diet is recommended while the patient recovers from the surgical procedure.

Table 1
Alloy design based on toxicological limit and biodegradation.

%	Element	Degradation days	Weight in g.	Complies for toxicology g. /days	Toxicological limit in g./days
69.18	Mg	150	20.75	0.140	0.700
4.99	Zn	150	1.49	0.010	0.015
25.83	Ca	150	7.74	0.052	0.800

In the biofabrication of this alloy, an induction furnace TF4000, INDUTHERM, Erwärmungsanlagen GmbH, Germany was used, conditions such as the heating ramp were determined from a series of experiments shown in figure 2, in foundry 1 and 2, the alloy was not homogenized, initiating an ignition process due to the high temperature and mainly attributed to the absence of the argon protective atmosphere during preheating and the casting process. Mg reactivity limits its use (64). Using flux (Melrasal) and the Ar atmosphere were the positive difference in casting 3, additionally the temperature and time parameters were adjusted, as shown in the curve. The homogenization period that allowed an adequate diffusion of the Zn powder on the MgCa master alloy corresponds to 36 min.

The induction smelting process considered the preheating of the smelting system to avoid humidity, inducing a reductive atmosphere of Argon (99,999) used to purge the interior of the Mg oxide crucible, prior to purging with argon, a second 244 ml 80 x 63 mm porcelain crucible with a lid was placed inside the Mg oxide crucible containing the charge of the elements Mg – 30 wt% Ca master alloy, Hunan, China and purified Zn, Fermont, US, these were completely covered with Flux (Melrasal UE, Magnesium elektron, UK), a flow of Argon (5 x 10^{-2} torr) was kept constant from the preheating process of the furnace until the porcelain crucible was extracted when cooling.

During the smelting process, using Argon will reduce evaporation, it is necessary to have a gas purification system which will reduce contraction, to homogenize the casting, the temperature was maintained for 36 minutes at 700 ° C, rapid solidification is recommended to increase strength, elongation and improve processability, this will allow an abrupt and ideal transition to cooling to form a smaller grain(65). The density of the alloy was calculated from the chemical composition and corresponds to 1.9534 Kg / m^3. Kumar et al reported that the limitations of Mg smelting are characterized by a precarious distribution of elements causing segregation and porosity (66). Avoiding the contact of the elements to be melted with other surfaces is of vital importance to avoid contamination with traces and impurities(48).

In the previously proposed formulation Mg – 25 wt% Ca + 5 wt% Zn, it is considered that increasing the Zn content by more than 1 wt% will reduce the amount of hydrogen formed in the reaction, Mg (s) + 2H2O ◊Mg (OH) 2 (aq) + H2 (g), which contributes to improving the corrosion rate(67)(68), exceeding the percentage of Zn by 5 wt% in the suggested chemical composition will increase the cytotoxic level which

will reduce cell viability. This alloy exhibits brittle behavior for which cold deformation treatments such as ECAP are suggested to increase its strength. Vinogradov et al, presented a study where severe plastic deformation refines the microstructure and produces a modification on the surface texture of Mg, improving the resistance(69)(70)(71)(72)(73)(74). Afandy et al, has reported that some mechanical treatments can nano-structure the surface of materials(75). Thermal stability depends on microstructural parameters, such as the composition of the phases (76). One of the biggest unknowns to date is the toxicological impact in vivo due to the size of a nanoparticle on the evolution of the pathophysiology reported for different chemical elements, this has a causal relationship between the quantity of elements and the release of nanoparticles to the organism.

Special care must be taken with heat treatments as these affect the corrosion rate, due to the intermetallic phases resulting from casting may dissolve. The weakening and random basal texture can be obtained after the annealing(77). Adding 1 wt% in Ca increases the tensile strength, the solubility of Ca in Mg is 1.34% wt at 789 ° K. The incorporation of Ca and Zn on Mg favors to increase the mechanical properties (30)(78)(79)(80)(81)(82)(83)(84)(85)(86)(87)(88)(89)(90)(91)(92)(93). Sergio Medina et al, present information on the complexity of strengthening MgCa alloys by heat treatment. Adding Ca will reduce the ignition point of Mg, however the hardness decreases when it exceeds 1.8 wt%(89)(94). Figure 3 shows the result of the third casting test of the alloy Mg − 25 wt% Ca + 5 wt% Zn.

Mg base alloy Mg – 25 wt% Ca + 5 wt% Zn (Magnesium: 63.19 wt%: Calcium: 25.03 wt%: Zinc: 5.18 wt%: Oxygen: 6.60 wt %) Obtained by atomic diffusion of Zn over MgCa, it is proposed for the manufacture of a porous scaffold, which must have mechanical and biological properties like DBM to be used as an alternative in pathologies related to orthognathic. The validation of cell viability, and its mechanical properties obtained under micro-indentation and techniques such as SEM-EDS, TEM and XRD must comply with what is related to ISO10993, evidencing a viable proposal. The behavior of the material is fragile due to the secondary phases and its lamellar morphology(95). Senkov et al, reported in their study that the CaMg2 phase has slow nucleation kinetics(65). Jardim et al, reported that this CaMg2 phase has a high melting point and is characterized by an adequate Intermetallic balance(96).

3 Methods

Several techniques such as SEM-EDS, XRD, TEM, micro-indentation and cell viability were combined to explain with a combinatorial approach the properties and behavior of the proposed alloy for a porous scaffold. The composition and formation of the phases originate the mechanical behavior, the detachment of the constituents from the alloy matrix modify the biological behavior depending on the concentration and release rate, having the information on the performance of the proposed alloy can help to understand its applicability in different pathologies as an alternative biomaterial. The use of Mg alloys has been suggested in applications where the load applied to the bone structure is minimal or very low, therefore applications in orthognathic surgery are a field of development for these materials(48).

3.1 SEM-EDS

The metallographic samples were roughened with 300–3000 sandpaper and polished with 0.3 μm alumina paste, in the microscope configuration, the filament and the current emission window were checked, the intensity was confirmed in 2, the sample is inserted into the holder and observation is carried out. The microscope is equipped with an energy dispersive spectrometer (EDS) to obtain the distribution of the elements in the microregions of interest and thus be able to confirm the diffusion. A metallographic preparation was performed on a specimen by performing a microscopy utilizing SEM-EDS, to reveal the morphology of the Mg – 25 wt% Ca + 5 wt% Zn alloy, it was performed with a microscope, Nanosem200-FEI, Netherlands, adhering the samples with a graphite tape to a sample holder, the micrograph and the analysis employing EDS were obtained in an atmosphere under vacuum, magnifications were obtained with a resolution of 10 μm. SEM-EDS analysis used configuration parameters that correspond to 20 KeV at a magnification of 1469.

3.2 XRD

The morphology of samples was characterized by X-ray diffraction (XRD). XRD results showed the formation of biocompatible phases of MgCa2 and magnesium oxide on the surface of alloy Mg–25 wt%Ca + 5 wt% Zn. Sourav Dutta et al, in their work show how the degradation of implants manufactured in Mg produces the release of Mg oxide, additionally it is presented how this compound is used by the human body in the recovery of bone fractures(97). X-ray diffraction analysis (XRD), using an equipment empyrean, Spain was used to evaluating the present phases of the Mg-25 wt%Ca + 5 wt% Zn alloy. The XRD analysis was acquired from 5-130° with a step size of 0.03 at 40 mA and 45 keV using Cu Kα radiation.

3.3 TEM-FIB

A lamella was prepared for TEM, through a focused ion beam (FIB) thinning from Gallium to approximately 60 nm, with a double beam system, FEI QUANTA 200 3D, Netherlands, it was mounted on a grid keeping it under vacuum even before observation, the lamella was placed in a holder inside the equipment (TEM, Titan 80-300-FEI, Netherlands) (Fig. 6). Gallium is a beneficial element in osteosynthesis, it inhibits bone resorption (98). The TEM operating conditions correspond to 300 keV & 380 magnification, with an aperture for condenser lens # 2 of 150, the exposure time corresponds to 1 s, in Fig. 7 the diffraction pattern of the Mg – 25 wt% Ca + 5 wt% Zn alloy is shown, in high vacuum conditions from 10^4 to 10, to achieve an uninterrupted flow of electrons, the images that are observed correspond to the diffraction of the selected area of the lamella, this corresponds to bright field and dark field. The FIB thinning technique aims to highlight the nano-structure and crystallography of metallic products of Mg (99).

The identification of the planes was carried out with the help of the list of indexed peaks of the diffraction charts of the International center for diffraction data (ICDD), for each phase relating the interplanar measurement of TEM looking for a coincidence with respect to 2 theta in the list of indexed peaks and thus relating it to the hkl planes.

3.4 Micro-indentation

Specimens for micro-indentation were previously prepared, polished, and mounted on a holder which has holes to allow its holding, the tests were carried out at room temperature, two small sections were analyzed longitudinally and transversely, both samples were embedded in a resin epoxy without use of vacuum. After being ground using abrasive papers of decreasing grit size (300, 800, and 3000 grit) under deionized water, with successively finer grades of alumina powder, the finest being 0.3 μm the specimens are cleaned ultrasonically to remove surface debris.

The micro-indentation cycle consists of adequately focusing the sample surface, adjusting the load-displacement, stabilizing the system, unloading on the sample, maintaining the load for a relatively longer time that allows the thermal derivative to be calculated and finally completing the download. This test was performed with a Berkovich type indenter.

Experiments elucidated here were conducted using a nanoindenter 50–00191 NHTX S/N, CSM instruments, the system makes small marks in precise positions on a sample surface and acquires the load-displacement of the diamond indenter using the Oliver and Pharr method, using parameters such as approach speed 6000 nm / min, delta slope contact 80%, acquisition rate 10 Hz, max load 20 mN, loading-unloading rate 200 mN/min, pause 1 s, poisson ratio 0.30. The samples are kept positioned in an x-y-z triad system relative to the microscope. The instrument is insulated in a cabin to allow thermal stability and suspended on a pneumatic anti-vibration table to protect the results from external vibrations.

3.5 Cell viability

Specimens were machined into small 3 x 3 x 15 mm bars to perform a cell viability evaluation, where it is sought to represent the morphological changes. All procedures were carried out under aseptic conditions and in a sterile environment, ensuring cell recovery, adherence, and progression towards the exponential growth phase(100). Extracts were obtained by the elution method according to ISO 10993-12. Samples of Mg – 25Ca – 5Zn were immersed into the cell culture medium for 24 h at 5% CO^2, 95% humidity, and 37 °C, with a fixed ratio of surface area to medium volume of 1.25 cm^2/ml.(101) Then extracts were collected and evaluated for impact in cell viability. Qing et al have propose using an indirect proliferation assay adapted from ISO-10993-5 (37). Using an alloy of MgCa combined with collagen would improve bone regeneration, confirming the biological safety of the material(102). The study presented corresponds to an evaluation of the cytotoxicity and cellular proliferation of L-929 cells. It is vitally important to avoid the concentration of Zn at a level of 80 μM, it has been reported to inhibit cell viability and cell proliferation(103)(104). These previous findings correspond and agree with what was proposed in this work, defining a toxicological criterion for the use of Zn in Mg.

The murine fibroblast cell line (L-929; CCL1) was purchased from the American Type Culture Collection. Tissue culture medium, fetal bovine serum (FBS), and supplements were obtained from Gibco (IL, USA). Dyes, phosphate buffered saline (PBS), and dimethyl sulfoxide were purchased from Sigma-Aldrich Chemical Co (MO, USA). L-929 fibroblasts were grown in DMEM with 10% FBS and 2 mM L-glutamine in 5% CO^2, 95% humidity at 37 ° C.

For the NRU method, cells were cultured in 96-well plates at a density of 1 e + 5 cells / well and pre-cultured for 24 hours to allow adaptation of the cells before adding the extracts. The five non-serial dilutions of extracts with culture media ranging from 10–100% were placed on cells in quadruplicate. The treatments with culture media were kept as a reference (100% viability). Zinc diethyldithiocarbamate (ZDC) 0.1% was used as a cytotoxic control.

After an incubation period of 48 hours, the 96-well plate was centrifuged (210 g for 10 minutes) and the medium was replaced by the neutral red spot (100 µl of a 0.2 mg / ml cell culture medium) in each well and the plate. It was incubated again at 37 ° C for 4 hours. The plate was then washed with PBS once and then removed, allowed to dry for 1 hour and 100 µl of neutral red eluent was added to each well. (Ethanol: dH2O: acetic acid 50:49:1). The plate was then shaken for 1 hour to dissolve the dye. After the neutral red dissolved, the absorbance was measured spectrophotometrically using a microplate reader (xMark, BioRad, USA) at a wavelength of 540 nm with a reference wavelength of 630 nm (38). According to ISO 10993-5: 2009, a relative metabolic activity of less than 70% was considered cytotoxic.

Negative controls included treatments with culture media. The cytotoxicity of 0.1% zinc diethyldithiocarbamate (ZDC) in culture media was evaluated under the same experimental conditions as the positive control. The cell viability was estimated by measuring the rate of mitochondrial reduction of tetrazolium-dye (MTT). The MTT assay determines the reduction of yellow soluble tetrazolium salt to an insoluble purple formazan crystal via a mitochondrial-dependent reaction only in metabolically active viable cells.

4 Results

The results obtained confirm the diffusion of Zn over the MgCa master alloy, Zn is not reflected in the composition of the phases due to inconsistencies in the sample and possibly the preferential orientation of the material. Interplanar distances could be identified and measured, Zn could be located when mapping by EDS, which suggests that the part analyzed by XRD did not contain Zn, which is attributed to the poor dispersion during solidification, however, it is not induced no change in cell viability as a product of Zn. There are some peaks that could not be identified by means of XRD, when crossing the information with the observation by TEM, it is verified that there is Zn in the sample, which suggests the formation of tiny crystalline phases of MgZn2.

4.1 SEM-EDS.

The mapping of elements is shown in Fig. 4 by means of a distribution analysis by SEM-EDS (O, Mg, Ca, and Zn). The main objective was the diffusion of Zn on the MgCa master alloy. There is a recrystallized microstructure with second phases in the matrix, without generalized homogenization due to the conditions of the casting process, in general there is no positive segregation of the elements, the diffusion of Zn on the MgCa master alloy is confirmed in the analysis by SEM-EDS. The lamellar morphology is very similar to that found in porous scaffolds for craniomaxillofacial reconstruction (CMF)

(105). Alshaaer et al, reported a pore size between 1-400 μm (13)(15)(32). Mayama et al, reported that under compression conditions, porous Mg has a high energy absorption efficiency (106)(19)(107).

4.2 XRD.

Identification of secondary phases was carried out by XRD, this alloy is composed of microstructural phases α-Mg, CaMg2 and MgO presented as a periclass, a cubic form of Mg oxide, it was not possible to detect any phase as a product of Zn. Mguni et al postulate in their experimentation that the periclass in the form of MgO detected by XRD crystallizes directly from nano-sheets.(108)(109)(110). The phases formed do not represent impurities that impair the cellular viability of the alloy (66).

Figure 5 shows the diffraction pattern and the identification of the CaMg2 and α-Mg phases, not all reflections agree with the MgCa2 phase, presenting a strong preferential orientation in the plane (1 2 3) and confirming that there are reflections that do not coincide with any compound of Mg, Ca, the most intense reflections without coincidence are those of the angles 52.63 and 73.85 theta.

Ramírez et al, reported a similar effect in a Mg-Zn-Al alloy, even though it may be due to the sensitivity limits of XRD, they reported a plane relationship to the MgO phase (15).

Zn is not present in the section of the sample analyzed by XRD diffraction, which suggests that it could be due to the preferential orientation of the sample. Fuzeng Ren et al, reported in their work that the addition of Zn inhibits the crystallization of hydroxyapatite compounds(111). Tripathy et al, presented evidence that solid solutions of Zn - Ca hydroxyapatite result in incoherent values in lattice constants and diffraction patterns (112)(113). There is a reduction in the degree of crystallization of the phases, increasing Zn and decreasing Ca in an Mg alloy will modify the network parameters a and c, which can be determined by the Rietveld refinement method.

Figura 5 Patrón de difracción Mg – 25 wt% Ca + 5 wt% Zn.

4.3 TEM

Shown in Fig. 6 are bright field and dark field images obtained by TEM in addition to the FIB preparation of a lamella for observation by TEM. Figure 7 shows the linear measurement of the rings of the resulting diffraction pattern, two patterns are shown to highlight the identification of all the phases previously detected by XRD, with the ring measurement it is directly related to the closest value corresponding to the interplanar distance, d(A) of the diffraction charts and indexing for each corresponding plane, this for the α-Mg, CaMg2 & MgO phases, respectively 01-1141, 13–0450 & 04-0829. Figures 8,9 and 10 show images of HRTEM and its interplanar measurement related to the phase diffraction plane.

Figure 8 shows HRTEM images, taken from the sites marked by A, B and C. Image A shows the measurement of the interplanar distance of the MgO phase, which corresponds to 2.106 Å in plane 2 0 0, at the 1 nm scale, the image was taken at 1.25 million magnification by the bright field technique. Image B shows the interplanar space d2 for the MgO phase and corresponds to 2.42 Å in the 1 1 1 plane. Image C shows the interplanar space 3 of the α-Mg phase Y corresponds to 2.60 Å in the plane 0 0 2.

It is observed in Fig. 9, HRTEM images, taken from the sites marked by A, B and C. Image A shows the measurement of the interplanar distance d6 of the α-Mg phase, which corresponds to 2.45 Å in the 1 0 1 plane, at the 1 nm scale. Image B shows the interplanar space d4 for the CaMg2 phase and corresponds to 2.29 Å in the 1 0 4 planes. Image C shows the interplanar space d5 of the CaMg2 phase and corresponds to 3.14 Å in the 1 1 0 plane.

It is observed in Fig. 10, HRTEM images, taken from the sites marked by A, B and C. Image A shows the measurement of the interplanar distance d7 of the CaMg2 phase, which corresponds to 2.87 Å in the 1 0 3 planes, at the 1 nm scale. Image B shows the interplanar space d8 for the CaMg2 phase and corresponds to 2.40 Å in the 2 0 2 planes. Image C shows the interplanar space d9 of the α-Mg phase and corresponds to 2.77 Å in the 1 0 0 plane.

4.4 Micro-indentation.

The mechanical properties of the Mg − 25 wt% Ca + 5 wt% Zn alloy were determined in the longitudinal and transverse direction using micro-indentation, 9 individual measurements for each direction were made to map the areas of the material due to the brittleness presented.

In Figs. 12 and 13, the force-penetration depth and force-indentation curves of the average measurement corresponding to the transverse direction are observed. These values correspond to Pmax: 20.46 mN, hmax: 481.75 nm, S: 0.2137 mN / nm, hc: 410.96 nm

4.5 Cell viability.

The Mg-25 wt% Ca + 5 wt% Zn alloy extracts did not induce any change or impact on cell viability or morphology, ruling out any detrimental effects. (See Fig. 14) The osmolality caused by Mg must be taken into account as an effect that will produce cellular stress(102).

It can be noted that in none of the serial solutions, including the concentration of 100% extract, there was a decrease in metabolic activity that affects cell viability, and this result verifies that the selection of elements for a biomedical alloy from the foundry, As stated at the beginning of this work, it is a key and avant-garde strategy for the development of new biomedical alloys, work is still needed to improve the mechanical properties. However, this result is an element of judgment that will contribute to achieve the sanitary regulation of Mg as a biomaterial for the manufacture of implants. Ramírez et al presented a definition of the natural process when selecting elements and called it bio-inspired design(15).

L-929 murine fibroblast experienced a not cytotoxic outcome in a dose-response fashion when exposed for 24 or 48 h to incremental concentrations of original extracts of Mg – 25 wt% Ca + 5 wt% Zn. (Fig. 15B) The effect extended of Mg – 25 wt% Ca + 5 wt% Zn extract on cell viability wasn´t comparable to that of cytotoxic molecule Zinc diethyldithiocarbamate (ZDC 0.1%) Fig. 14. There was no rounded or lised in the cells, monolayers and a growth are observed. While in the cell cultures exposed to Mg – 25 wt% Ca + 5 wt% Zn extracts there is cell adhesion, but not evident intracytoplasmic granules and morphological changes, the % growth inhibition is observed. The Mg – 25 wt% Ca + 5 wt% Zn extracts did not induce any reduction in cell viability not in cell morphology, discarding any detrimental effect on cells.

The cell metabolic activity (viability) of adhered L-929 cells exposed to Mg – 25 wt% Ca + 5 wt% Zn original extracts was compared to untreated cells (negative control; CTRL) and cells treated with the cytotoxic Zinc diethyldithiocarbamate (ZDC) after two days of same culture conditions.

4.6 Validation by Finite Element Method, load progression versus comparison to BDM.

A FEM simulation was performed using Ansys 15 software to visualize the mechanical behavior of the alloy and its response to failure modes. An isotropic bi-linear simulation was performed creating the material Mg – 25 wt% Ca + 5 wt% Zn, the properties used were Young´s modulus 74.2 GPa (Longitudinal), Poisson 0.30 (obtained by micro-indentation), using a uniaxial table to tabulate the behavior of the material. Tensile yield strength was configured at 50 MPa and tensile strength ultimate at 290 MPa the deformation that the material can withstand corresponds to 0.017 mm/mm.(84) The model consists of 30887 nodes and 17779 SOLID 186 elements; large deflection was activated to control deformation. The boundary conditions were 1 fixed support on the lateral face and application of compressive force by 8.31 N. The maximum elastic deformation was .01703 mm/mm, while the maximum stress that it supports before failure corresponds at 0.447 MPa. When comparing these values with the mechanical properties of the DBM, is that it is verified that the proposed alloy Mg – 25 wt% Ca – 5 wt% Zn can be used as a viable alternative to replace cadaver bone, from the perspective of biocompatibility, the elements used and the products of the phases created do not represent a cytotoxic effect according to with ISO-10993, Mg, Ca and Zn have been related as elements that promote osseointegration and osteogenesis. Sudeep Paul, Anvari-Yazdi et al, demonstrated that elements such as Ca and Zn have a neutral effect on adipose-derived mesenchymal stem cells(114)(115). Chaoxing Zhang et al, demonstrated that Mg - Zn - Ca alloys possess antimicrobial properties and are promising options in bone repair(116)(21). Rahman et al report that Mg base alloys can be enriched with antibiotics to improve their antibacterial performance(4)(15)(117)(118)(119).

5 Discussion

Starting the process from a master alloy with the approximate percentages of the desired composition will be the best alternative due to economic-environmental viability for casting Mg alloys for biomedical purposes.

Regarding the release of harmful ions, Cicha et al, propose to use ferritic elements for cardiovascular applications, this in order to be able to recover dissolved metal ions with adherence of endothelial cells by magnetism and to evaluate the therapeutic benefit(120)(121). When using Mg base alloys, this would not be possible mainly due to Mg ions due to their characteristic paramagnetic, if this study phenomenon is of interest, a good strategy would be to dope Mg with elements such as Nd to promote a partial recovery of ions metallic where the effect on Nd ions can be sampled. An advantage of its use is that Nd acts as a grain refiner, contributing to mechanical integrity, however its toxicological potential has limited its use in medical devices (122)(123), a possible alternative to use it at an exposure limit with biosecurity precautions could be implemented through the magnetic cell recruitment technique proposed by Cicha.

The contribution of the MgCa2 phase to the mechanical behavior of the alloy is related to the morphology of the eutectic lamellar phase providing the characteristic brittleness and has the implication that the melting point of the phase is below the melting point of both main constituents., the solidification of interlocking sheets explains the nature of brittleness in the material. The development and medical use of Mg alloys have been limited due to the poor formation of sliding systems that induce low ductility, becoming more complicated when adding elements to reinforce the matrix of the alloy(97). Adding pure elements such as Ca and Zn to form this base-Mg alloy will be restricted due to the solubility limits of the elements. Understanding the formation of each of the phases and checking the preferential orientation of the grain in the morphological characterization would indicate the affectation of Mg alloys when transformed by fusion or mechanical deformation, providing evidence that dynamic recrystallization occurs(124)(125). Park et al, have reported that both plastic deformation and the atomic diffusion process induce preferential orientation of the grain(126). The existence of diffuse diffraction rings is an indicator of the replacement of Mg ions by Ca, there was variation in intensity and circumference, this phenomenon was also reported by Bowen(99). The crystalline orientation (texture) has an impact on the degradation of Mg alloys (127). This impact is greater in the application, if the flow of the body fluid affects the normal orientation to the surface, when the surface of the Mg is exposed to the flow of a body fluid, the bio-erosion produced by the fluid influencing the material accelerates the degradation, to prolong the life of a Mg implant, it should be recommended in surgical techniques to take care of the placement, avoiding as much as possible that the implant is exposed to a blood flow that affects perpendicularly on the surface, considering this effect can improve the performance of a medical device manufactured in Mg. Deepening the characterization of the texture of a MgCa implant depends largely on the behavior of the alloy, even when the texture is improved, the behavior of MgCa alloys will show tendencies towards brittleness.(128)(129). Various efforts have been made to improve the casting process and consequently the mechanical properties of MgCa alloys(48). However, no matter how much the process can be improved, it must be considered that the eutectic lamellar phases that originate will always be present in the incorporation of Ca to Mg, the homogenization due to the improvements in foundry offers to improve the biocompatibility(130)(131)(132)(133), however the characteristics of the morphologies reported indicate a strong inclination towards fragility.

The mechanical properties are also affected due to the orientation of the grain, causing microstructural changes due to the elongation of the grains themselves and this is reflected in their elastic components, inducing anisotropy(134)(135)(136)(137)(138).

The combination of SEM-EDS, XRD & TEM techniques allow us to understand the importance of each microstructural phase and its effect. Twins within the grains can prevent band dislocations and are related to material creep. The α-Mg phase normalizes the MgCa2 matrix and prevents acceleration in degradation(139).

In Fig. 4a non-homogenized morphology can be seen, and it is logical since the ideal is to melt these materials under vacuum and centrifuge them, however, a diffusion of Zn over MgCa is achieved, which is

the most important part of the work because allows us to carry out the evaluation of cell viability directly from the material.

Traces of pitting corrosion were observed during the SEM-EDS analysis that indicate that the alloy is resistant to corrosion, however, this corrosion will act as a stress concentrator and the degradation process will start as soon as the material is superficially affected. affecting the mechanical properties and leading to eventual dissolution(140). The distribution of mechanical stresses is not homogeneous throughout the material due to the crystallographic orientation and the second phases that initiate the nucleation of the material, also generating cracks, pores, and precipitates. Cesarz et al, reported that dissolved Ca particles can precipitate and form anticorrosive layers that slow down degradation (141) (142).

It is possible that Zn is not detected because there are only small amounts in the alloy, however, it has already been reported that in Mg-Zn diffraction, only the α-Mg phase diffracts intensity, Yan Jingli, reported that by decreasing the Scanning speed during XRD analysis, the formation of weak diffraction peaks of the MgZn2 phase is revealed, such as those formed and not identified in the result shown for XRD (See Fig. 5). The lack of identification of Zn phases can be attributed to multiple causes, including a possible preferential reorientation during the preparation of the specimens, unfortunately Yan Jingli does not report a scanning speed for the detection of the MgZn2 phases by XRD, the value used in this work corresponds to scan step time [s], 59.69, which suggests that a lower speed should be used. An atomic rearrangement by a mechanism such as hardening deformation will increase the intensity of Zn (128). The structured lattice arrangement in the generation of quasicrystalline phases has shown excellent mechanical properties, reducing the coefficient of friction and resistance to corrosion (143).

This alloy shows a phenomenon due to precipitates where the Zn peaks do not appear, it could be partly that a rearrangement is required and what existed was a preferential orientation due to the sanding process, when polishing the sample or When the elements were melted, they were superficially deposited and agglomerated, which causes them to be removed with sandpaper when polishing or a preferential reorientation occurs.

Avoid increasing the temperature above 200 ° C on the surface of an implant made of MgZn alloy, this will minimize microstructural modification (56)(144). Galvanic corrosion that occurs between Mg and Zn generates a rapid dissolution of secondary phases, weakening the Mg matrix, this explains the potential for bioactivity generated by these elements acting together in an alloy.

Tripathy, reported that solid Zn-Ca solutions could be prepared in the entire range of compositions, although incoherent values of the grating parameters and diffraction patterns were observed, through the study by the ritveld method it was determined that the parameters change when adding Zn existing a modification(113)(111).

The results shown correspond to the average value of 9 tests for longitudinal and transverse orientation, in the upper half of the load vs displacement curve are the data with which the elastic modulus (E) and

hardness H (VK) are calculated.), during load application, elastic and plastic deformations occur under the indenter as the contacts change deeper. The discharge part of the curve is dominated by elastic displacements. The diamond indenter has a V = 0.07 and an E = 1140 GPa, the MgCa-Zn material has a V = 0.30, through sensivity studies it has been determined that variations in the range of 0.2–0.4 in V, will present a variation the elastic modulus E not greater than 8%.

The determination of the elastic modulus derived from the Oliver and Pharr method consists of an average of the isotropic elastic constants, however, for an anisotropic material it has been determined that the measurements are inclined towards the elastic modulus in the direction of the test. For a material that exhibits an HCP structure, the determination of the elastic modulus only considers the normal direction, underestimating the other elastic components by mono-crystallinity, the influence of the elastic constants that occur in an orthotropic material are of vital importance for understand the behavior of the material.

Fibroblasts tend to adhere to the surface and show an elongated polygonal morphology, this if they are healthy and normal. And if they present a degraded appearance and spherical morphology in addition to the detachment of the surface, they usually indicate cell death, which is not observed.

As complementary perspectives to cell viability it is widely recommended to use analyzes that represent cell dynamics by monitoring cell properties in real time, it is desired know the adherence to non-foulding surfaces, proliferation, and cell migration(145)(146)(147)(148)(149).

Viz, Yang et al reported an increase in cell viability of osteoblasts reducing DNA damage in the formation of new bone using Zn-Mg alloys (150)

Conclusion

As a general conclusion

1. The optimization of the casting process of a Mg-Ca-Zn alloy has a microstructural limit, which is due to the eutectic mixture, even when the process is optimized, a fine dispersion between phases will continue to appear, resulting in an origin for crack nucleation.
2. The period of exposure to elements such as Mg, Ca and Zn within the body causes pathophysiology to occur, being clear about the period of exposure in days for the effects to occur is a key factor to understand the beneficial effect that they can contribute prior to hydrolytic degradation in vivo.
3. Zn improves the mechanical response when hardening this type of alloys, however, exceeding the permitted limits damages the toxicological limit which will have an impact on cell viability. Viz, Zhuang, et al reported Zn dose-dependent and over-boosted concentration caused cell death due to cytotoxicity(103). Elements such as Sr and Ca have been reported to be able to counteract and reduce the toxicity of Zn (151)(152). Lu et al reported that Zn promotes the absorption of the hydrogen that is released due to the Mg reaction in vitro (153).

4. An annealing process on this alloy will dissolve the intermetallic phases that occur and help to homogenize the distribution of the solutes in the Mg matrix, however, the precipitates could have a detrimental effect on the corrosion rate.
5. The melting of Mg, Ca and Zn and their modification by diffusion are possible from MgCa master alloys, this process manages to diffuse Zn in powder over MgCa, the use of a vacuum system will allow to have a clean atmosphere. The alloy microstructure and grain size will be finer.
6. The coatings on Mg alloys are very important depending on the type of medical application for which they are required to be used, a coating used on Mg alloys has the purpose of increasing the implant time in vivo, that will provide mechanical resistance to the fracture, for this application, using a coating that reduces the appearance of pitting corrosion is a multidisciplinary strategy that will completely depend on the initial weeks in which it is required to maintain the mechanical integrity of the implant, it is suggested to evaluate a coating based on Chitosan that allows to maintain implant surface intact for 6 weeks to minimize places where crack propagation can begin.
7. The elastic modulus was 74.2 GPa for the longitudinal direction and 66.2 GPa in the transverse direction, it has been determined from the repetitions of the test that the elastic modulus was always higher in the longitudinal direction, the hardness follows a similar pattern being reported 278.9 and 264.3 HV in longitudinal and transverse direction, respectively. An anisotropy condition between the longitudinal and transverse direction is fulfilled by having different elastic modulus and hardness. The determination of the elastic modulus and hardness in each triad for each degree of freedom could be useful to relate to the orientation of the planes and to have the behavior of the elastic constants characterized.
8. The ideal application for this type of alloy corresponds to anatomical sites where it is only exposed to gravity and forces caused by muscles such as the movement of the upper extremities and the skull.
9. Experimenting with texture control techniques on Mg alloys could be an effective strategy to determine the ideal method for manufacturing Mg-based implants. However, the mechanical behavior of Mg depends on the adequate relationship between the volumetric fraction of elements and the formation of lamellar long period stacking order (LPSO) secondary phases.(144)(154)(155).

List Of Abbreviations

Magnesium (Mg), Calcium (Ca), Zinc (Zn), Demineralized bone matrix (DBM), American Association of Tissue Banks (AATB), Bone morphogenetic protein (BMP), Craniomaxillofacial (CMF), Long period stacking order (LPSO)

Declarations

It is declared by the authors of this work that there is no conflict of interest regarding the following.

Ethics approval and consent to participate: N/A

Consent for publication: N/A

Availability of data and materials: OK

Competing interests: No conflict of interest.

Funding: N/A

Authors' contributions

LHCB, He contributed to the writing of the document, elaboration of the selection process of elements and conduction of the casting process, sample preparation and facilities for the rest of the essays presented in the manuscript.

MALRH, contributed to the structure of the document.

JPL, Support in the casting process from the preparation of molds in each of the castings carried out to the weighing and loading of the elements.

RLA, He provided the elements Mg, Ca, and Zn for experimentation, took over the mechanical review of the tests.

HES, analyzed and interpreted the cell viability data regarding the test presented.

ATC, He performed the analysis of the samples by SEM-EDS, TEM, supporting the documentation of this manuscript, provided equipment to perform the experimentation by micro-indentation

ENP, He contributed to the search for information regarding the phenomena presented and in the writing of the document.

The authors state that they can share any information requested during the peer review process in the same way during the manuscript acceptance process.

Conflicts of interest

The authors declare that there is no conflict of interest regarding the publication of this paper.

Acknowledgments

Thanks to Hugo Esquivel Solis and CIATEJ, for the unconditional support to perform biological tests on specimens and for their objective view of the work. Thanks to CIQA and Enrique Díaz Barriga for their support in preparing the FIB samples for crystallographic analysis. Thanks to Dr. Arturo Juarez for the advice provided during the casting process.

References

1. Fischer J, Feyerabend F, Hort N, Kainer KU, Schreyer A. Cytotoxic and Immunological Effects of Magnesium Alloy Ele- ments on Cells.
2. Chen X. Magnesium-based implants: Beyond fixators. J Orthop Transl. 2017;10:1–4.
3. Holweg P, Berger L, Cihova M, Donohue N, Clement B, Schwarze U, et al. A lean magnesium–zinc–calcium alloy ZX00 used for bone fracture stabilization in a large growing-animal model. Acta Biomaterialia. 2020. 0–66 p.
4. Rahman M, Li Y, Wen C. HA coating on Mg alloys for biomedical applications: A review. J Magnes Alloy [Internet]. 2020;8(3):929–43. Available from: https://doi.org/10.1016/j.jma.2020.05.003.
5. Thouas GA. Metallic implant biomaterials. Mater Sci Eng R Reports. 2015;87:1–57.
6. Milenin A, Kustra P. Production of zinc wire for use as a high strength biodegradable surgical threads. In: Procedia Manufacturing. 2020. p. 757–60.
7. Milenin A, Kustra P, Byrska-Wójcik D, Wróbel M, Packo M, Sulej-Chojnacka J, et al. Production of zinc wire for use as a high strength biodegradable surgical threads. Procedia Manuf. 2020;50(September):757–60.
8. Parfenov EV, Kulyasova OB, Mukaeva VR, Mingo B, Farrakhov RG, Cherneikina YV, et al. Influence of ultra-fine grain structure on corrosion behaviour of biodegradable Mg-1Ca alloy. Corros Sci. 2020;163(October).
9. Pulido-gonzález N, Torres B, Rodrigo P, Hort N, Rams J. Microstructural, mechanical and corrosion characterization of an as-cast Mg – 3Zn – 0. 4Ca alloy for biomedical applications. J Magnes Alloy. 2020;(xxxx).
10. Holtzclaw D, Toscano N, Eisenlohr L, Callan D. The safety of bone allografts used in dentistry: A review. J Am Dent Assoc. 2008;139(9):1192–9.
11. Salyer KE, Taylor DP. Bone grafts in craniofacial surgery. Clin Plast Surg. 1987;14(1):27–35.
12. Wang JC, Alanay A, Mark D, Kanim LEA, Campbell PA, Dawson EG, et al. A comparison of commercially available demineralized bone matrix for spinal fusion. Eur Spine J. 2007;16(8):1233–40.
13. Maier HJ, Julmi S, Behrens S, Klose C, Gartzke AK, Wriggers P, et al. Magnesium Alloys for Open-Pored Bioresorbable Implants. Jom. 2020;72(5):1859–69.
14. Liu C, Ren Z, Xu Y, Pang S, Zhao X, Zhao Y. Biodegradable Magnesium Alloys Developed as Bone Repair Materials: A Review. Scanning. 2018;2018.
15. Ramirez Patino JF. Bioresorbable magnesium-based sponge and foam materials. Methods and devices [Internet]. World Intellectual Property Organization International Bureau. World Intellectual Property Organization; WO 2018/187756 Al, 2018. Available from: https://doi.org/10.1016/j.idcr.2017.10.009%0Ahttp://www.mendeley.com/research/geology-volcanic-history-eruptive-style-yakedake-volcano-group-central-

japan/%0Ahttps://doi.org/10.1186/s13068-018-1170-4%0Ahttps://doi.org/10.1186/s13068-019-1512-x%0Ahttps://d.

16. Campos Becerra LH, Esquivel Solís HRM, Lesso Arroyo H, Torres Castro R. A. Bio-inspired biomaterial Mg-Zn-Ca: a review of the main mechanical and biological properties of Mg-based alloys. Biomed Phys Eng Express. 2020 May.
17. Li X, Niu Y, Guo H, Chen H, Li F, Zhang J, et al. Preparation and osteogenic properties of magnesium calcium phosphate biocement scaffolds for bone regeneration. J Instrum. 2013;8(7).
18. Deng J, Ye J, Zhao Y, Zhu Y, Wu T, Zhang C, et al. ZnO and Hydroxyapatite-Modified Magnesium Implant with a Broad Spectrum of Antibacterial Properties and a Unique Minimally Invasive Defined Degrading Capability. ACS Biomater Sci Eng. 2019;5(9):4285–92.
19. Alshaaer M, Abdel-Fattah E, Saadeddin I, Battah F, Al, Issa K, Saffarini G. The effect of natural fibres template on the chemical and structural properties of Biphasic Calcium Phosphate scaffold. Mater Res Express. 2020;7(6).
20. Ehsanollah Moradi M, Ebrahimian-Hosseinabadi M, Khodaei ST. Magnesium/Nano-Hydroxyapatite porous biodegradable composite for biomedical applications. Mater Res Express. 2019;in press:0–31.
21. Ong KL, Yun BM, White JB. New biomaterials for orthopedic implants. Orthop Res Rev. 2015;7(September 2015):107–30.
22. U.S Food & drug administration. Jurisdictional Update: Human Demineralized Bone Matrix. 2018.
23. Wang JL, Xu JK, Hopkins C, Chow DHK, Qin L. Biodegradable Magnesium-Based Implants in Orthopedics—A General Review and Perspectives. Adv Sci. 2020;7(8).
24. Gao C, Peng S, Feng P, Shuai C. Bone biomaterials and interactions with stem cells. Bone Res [Internet]. 2017;5(May):1–33. Available from: http://dx.doi.org/10.1038/boneres.2017.59.
25. Amerstorfer F, Fischerauer SF, Fischer L, Eichler J, Draxler J, Zitek A, et al. Long-term in vivo degradation behavior and near-implant distribution of resorbed elements for magnesium alloys WZ21 and ZX50. Acta Biomater. 2016;42:440–50.
26. Lesz S, Kraczla J, Nowosielski R. Structure and compression strength characteristics of the sintered Mg–Zn–Ca–Gd alloy for medical applications. Arch Civ Mech Eng [Internet]. 2018;18(4):1288–99. Available from: https://doi.org/10.1016/j.acme.2018.04.002.
27. Bakhsheshi-Rad HR, Abdellahi M, Hamzah E, Ismail AF, Bahmanpour M. Modelling corrosion rate of biodegradable magnesium-based alloys: The case study of Mg-Zn-RE-xCa (x = 0, 0.5, 1.5, 3 and 6 wt%) alloys. J Alloys Compd. 2016;687:630–42.
28. Wang Y, Liu G, Wei Y, Qiao Y. Effects of Magnesium-Calcium Alloys with Different Calcium Content on Their Mechanical Properties. IOP Conf Ser Mater Sci Eng. 2020;735:012010.
29. Sezer N, Evis Z, Kayhan SM, Tahmasebifar A, Koç M. Review of magnesium-based biomaterials and their applications. J Magnes Alloy. 2018;6(1):23–43.

30. Radha R, Sreekanth D. Insight of magnesium alloys and composites for orthopedic implant applications – a review. J Magnes Alloy. 2017;5(3):286–312.
31. Thomas O, Xu HS, Kim, Tyler Stahl SPN. Self-neutralizing PLGA/magnesium composites as novel biomaterials for tissue engineering. Biomed Mater. 2018;in press:0–31.
32. Alshaaer M, Abdel-Fattah E, Saadeddin I, Battah F, Al, Issa K, Saffarini G. The effect of natural fibres template on the chemical and structural properties of Biphasic Calcium Phosphate scaffold. Mater Res Express. 2020;7(6):065405.
33. Gu XN, Li N, Zhou WR, Zheng YF, Zhao X, Cai QZ, et al. Corrosion resistance and surface biocompatibility of a microarc oxidation coating on a Mg-Ca alloy. Acta Biomater. 2011;7(4):1880–9.
34. Sedelnikova MB, Komarova EG, Sharkeev YP, Tolkacheva TV, Sheikin VV, Egorkin VS, et al. Characterization of the Micro-Arc coatings containing β-tricalcium phosphate particles on Mg-0.8Ca alloy. Metals (Basel). 2018;8(4):1–15.
35. Farahany S, Bakhsheshi-Rad HR, Idris MH, Abdul Kadir MR, Lotfabadi AF, Ourdjini A. In-situ thermal analysis and macroscopical characterization of Mg-xCa and Mg-0.5Ca-xZn alloy systems. Thermochim Acta [Internet]. 2012;527:180–9. Available from: http://dx.doi.org/10.1016/j.tca.2011.10.027.
36. Zeng R, Lan Z, Kong L, Huang Y, Cui H. Characterization of calcium-modified zinc phosphate conversion coatings and their influences on corrosion resistance of AZ31 alloy. Surf Coatings Technol [Internet]. 2011;205(11):3347–55. Available from: http://dx.doi.org/10.1016/j.surfcoat.2010.11.027.
37. Qing Yu, Wang C, Yang J, Changwu Guo SZ. Mineralized collagen/Mg-Ca alloy combined scaffolds with improved biocompatibility for enhanced bone response following tooth extraction. Biomed Mater. 2018;13(6):1–23.
38. Feyerabend1 F, Witte2 F, Vogt2 C, Fischer1 J. A. Schreyer1, K. U. Kainer1, N. Hort1 RW. In Vitro Testing of Magnesium Alloys - Challenges and Options. Wiley-VCH Books.
39. Sharma P, Chattopadhyaya S, Singh NK. A review on magnetically supported gas metal arc welding process for magnesium alloys. Mater Res Express. 2019;6(8).
40. Toghyani S, Khodaei M. Fabrication and characterization of magnesium scaffold using different processing parameters. Mater Res Express. 2018;5(3).
41. Guan RG, Cipriano AF, Zhao ZY, Lock J, Tie D, Zhao T, et al. Development and evaluation of a magnesium-zinc-strontium alloy for biomedical applications - Alloy processing, microstructure, mechanical properties, and biodegradation. Mater Sci Eng C. 2013;33(7):3661–9.
42. Annur D, Franciska P, Erryani A, Amal MI, Sitorus LS, Kartika I. The synthesis and characterization of Mg-Zn-Ca alloy by powder metallurgy process. AIP Conf Proc. 2016;1725(April 2016).
43. Jin C, Narayan RJ. Structural and optical properties of hexagonal Mg xZn 1-xO thin films. J Electron Mater. 2006;35(5):869–76.
44. Mironov V, Trusk T, Kasyanov V, Little S, Swaja R, Markwald R. Biofabrication. A 21st century manufacturing paradigm. Biofabrication. 2009;1(2).

45. Ni M, Niu W, Wong DWC, Zeng W, Mei J, Zhang M. Finite element analysis of locking plate and two types of intramedullary nails for treating mid-shaft clavicle fractures. Injury. 2016;47(8):1618–23.
46. Senkov ON, Scott JM. Glass forming ability and thermal stability of ternary Ca-Mg-Zn bulk metallic glasses. J Non Cryst Solids. 2005;351(37–39):3087–94.
47. Gu X, Zheng Y, Zhong S, Xi T, Wang J, Wang W. Corrosion of, and cellular responses to Mg-Zn-Ca bulk metallic glasses. Biomaterials. 2010;31(6):1093–103.
48. Geanta V, Voiculescu I, Kelemen H, Manu D, Molnár G, Kelemen G. Mg-Ca-Zn bio-degradable light alloys produced in a levitation induction melting furnace. Int J Appl Electromagn Mech. 2020;63(S1):69–78.
49. Hrapkowicz B, Lesz ST. Characterization of Ca 50 Mg 20 Zn 12 Cu 18 Alloy. Arch Foundry Eng. 2019;19(1):75–82.
50. Ma S, Xing F, Ta N, Zhang L. Kinetic modeling of high-temperature oxidation of pure Mg. J Magnes Alloy. 2020;8(3):819–31.
51. Shahri Z, Allahkaram SR, Soltani R, Jafari H. Optimization of plasma electrolyte oxidation process parameters for corrosion resistance of Mg alloy. J Magnes Alloy. 2020;8(2):431–40.
52. Kumar A, Pandey PM. Development of Mg based biomaterial with improved mechanical and degradation properties using powder metallurgy. J Magnes Alloy. 2020;8(3):883–98.
53. Yang M, Liu D, Zhang R, Chen M. Microstructure and Properties of Mg-3Zn-0.2Ca Alloy for Biomedical Application. Xiyou Jinshu Cailiao Yu Gongcheng/Rare Met Mater Eng [Internet]. 2018;47(1):93–8. Available from: http://dx.doi.org/10.1016/S1875-5372(18)30078-X.
54. Smith CE. Aggie Digital Collections and Scholarship Processing And Characterization Of Innovative Magnesium Alloys For Biodegradable Orthopaedic Implants. 2015.
55. Bell S, Ajami E, Davies JE. An improved mechanical testing method to assess bone-implant anchorage. J Vis Exp. 2014;(84):1–10.
56. Fischerauer SF. Preclinical Characterization of Bioresorbable Magnesium Implants for. 2015.
57. Liu C, Wang J, Gao C, Wang Z, Zhou X, Tang M, et al. Enhanced osteoinductivity and corrosion resistance of dopamine/gelatin/rhBMP-2–coated β-TCP/Mg-Zn orthopedic implants: An in vitro and in vivo study. PLoS One [Internet]. 2020;15(1):1–24. Available from: http://dx.doi.org/10.1371/journal.pone.0228247.
58. Hiromoto S, Itoh S, Noda N, Yamazaki T, Katayama H, Akashi T. Osteoclast and osteoblast responsive carbonate apatite coatings for biodegradable magnesium alloys. Sci Technol Adv Mater. 2020;21(1):346–58.
59. Chang YH, Tseng CC, Chao CY, Chen CH, Lin SY, Du JK. Mg-Zn-Ca alloys for hemostasis clips for vessel ligation: In vitro and in vivo studies of their degradation and response. Materials (Basel). 2020;13:13.
60. Sarkar K, Kumar V, Devi KB, Ghosh D, Nandi SK, Roy M. Anomalous in Vitro and in Vivo Degradation of Magnesium Phosphate Bioceramics: Role of Zinc Addition. ACS Biomater Sci Eng.

2019;5(10):5097–106.

61. Ostrowski N, Lee B, Hong D, Enick PN, Roy A, Kumta PN. Synthesis, Osteoblast, and Osteoclast Viability of Amorphous and Crystalline Tri-Magnesium Phosphate. ACS Biomater Sci Eng. 2015;1(1):52–63.
62. Ibrahim H, Esfahani SN, Poorganji B, Dean D, Elahinia M. Resorbable bone fixation alloys, forming, and post-fabrication treatments. Mater Sci Eng C. 2017;70:870–88.
63. Gao JH, Guan SK, Chen J, Wang LG, Zhu SJ, Hu JH, et al. Fabrication and characterization of rod-like nano-hydroxyapatite on MAO coating supported on Mg-Zn-Ca alloy. Appl Surf Sci. 2011;257(6):2231–7.
64. Sharma P, Chattopadhyaya S, Singh NK. A review on magnetically supported gas metal arc welding process for magnesium alloys. Mater Res Express. 2019;6(8).
65. Senkov ON, Scott JM. Glass forming ability and thermal stability of ternary Ca-Mg-Zn bulk metallic glasses. J Non Cryst Solids. 2005;351(37–39):3087–94.
66. Kumar A, Pandey PM. Development of Mg based biomaterial with improved mechanical and degradation properties using powder metallurgy. J Magnes Alloy. 2020;8:883–98.
67. Xin Y, Hu T, Chu PK. Influence of Test Solutions on In Vitro Studies of Biomedical Magnesium Alloys. J Electrochem Soc. 2010;157(7):C238.
68. Yan Y, Chu X, Luo X, Xu X, Zhang Y, Dai YL, et al. A homogenous microstructural Mg-based matrix model for orthopedic application with generating uniform and smooth corrosion product layer in Ringer's solution: Study on biodegradable behavior of Mg-Zn alloys prepared by powder metallurgy as a case. J Magnes Alloy [Internet]. 2020;(xxxx). Available from: https://doi.org/10.1016/j.jma.2020.03.010.
69. Vinogradov A, Vasilev E, Kopylov VI, Linderov M, Brilevesky A, Merson D. High performance fine-grained biodegradable Mg-Zn-Ca alloys processed by severe plastic deformation. Metals (Basel). 2019;9(2).
70. Priyanto TH, Insani A, Muslih R, Bharoto. Texture Analysis on the AZ31 Magnesium Alloy Using Neutron Diffraction Method. J Phys Conf Ser. 2020;1436(1).
71. Park M, Kim K. Basal texture formation behavior of M1 magnesium alloy during high-temperature compression deformation. J Phys Conf Ser. 2019;1270(1).
72. Xie J, Zhang J, You Z, Liu S, Guan K, Wu R, et al. Towards developing Mg alloys with simultaneously improved strength and corrosion resistance via RE alloying. J Magnes Alloy. 2020;(xxxx).
73. Du P, Furusawa S, Furushima T. Microstructure and performance of biodegradable magnesium alloy tubes fabricated by local-heating-assisted dieless drawing. J Magnes Alloy. 2020;8(3):614–23.
74. Shi ZZ, Chen HT, Zhang K, Dai FZ, Liu XF. Crystallography of precipitates in Mg alloys. J Magnes Alloy. 2020;(xxxx):1–16.
75. Afandi R, Sutiyoko L. Characteristic modifications of magnesium and its alloy for future implant material - Review. J Phys Conf Ser. 2020;1517(1).

76. Janeček M, Krajňák T, Minárik P, Čížek J, Stráská J, Stráský J. Structural stability of ultra-fine grained magnesium alloys processed by equal channel angular pressing. IOP Conf Ser Mater Sci Eng. 2017;194(1).
77. Zheng M, Xu G, Liu D, Zhao Y, Ning B, Chen M. Study on the Microstructure, Mechanical Properties and Corrosion Behavior of Mg-Zn-Ca Alloy Wire for Biomaterial Application. J Mater Eng Perform. 2018;27(4):1837–46.
78. Kim Y-H, Yoo H-S, Son H-T. Microstructure and Mechanical Properties of Mg–11Li–6Zn–0.6Zr–0.4Ag–0.2Ca–x Y Alloys. J Nanosci Nanotechnol. 2018;18(9):6304–8.
79. Song G. Control of biodegradation of biocompatable magnesium alloys. Corros Sci. 2007;49(4):1696–701.
80. Hamidi MFFA, Harun WSW, Samykano M, Ghani SAC, Ghazalli Z, Ahmad F, et al. A review of biocompatible metal injection moulding process parameters for biomedical applications. Mater Sci Eng C. 2017;78:1263–76.
81. Vlcek M, Lukác F, Kudrnová H, Smola B, Stulíková I, Luczak M, et al. Microhardness and in vitro corrosion of heat-treated Mg-Y-Ag biodegradable alloy. Materials (Basel). 2017;10(1).
82. Li Z, Gu X, Lou S, Zheng Y. The development of binary Mg-Ca alloys for use as biodegradable materials within bone. Biomaterials. 2008;29(10):1329–44.
83. Cha P-R, Han H-S, Yang G-F, Kim Y-C, Hong K-H, Lee S-C, et al. Biodegradability engineering of biodegradable Mg alloys: Tailoring the electrochemical properties and microstructure of constituent phases. Sci Rep. 2013;3(1):2367.
84. Li YC, Li MH, Hu WY, Hodgson PD, Wen CE. Biodegradable Mg-Ca and Mg-Ca-Y Alloys for Regenerative Medicine. Mater Sci Forum. 2010;654–656(October 2015):2192–5.
85. Li T, He Y, Zhang H, Wang X. Microstructure, mechanical property and in vitro biocorrosion behavior of single-phase biodegradable Mg-1.5Zn-0.6Zr alloy. J Magnes Alloy. 2014;2(2):181–9.
86. Prakasam M, Locs J, Salma-Ancane K, Loca D, Largeteau A, Berzina-Cimdina L. Biodegradable Materials Metallic Implants—A Review J Funct Biomater. 2017;8(4):44.
87. Lu Y, Bradshaw AR, Chiu YL, Jones IP. Effects of secondary phase and grain size on the corrosion of biodegradable Mg-Zn-Ca alloys. Mater Sci Eng C. 2015;48:480–6.
88. Sikora-Jasinska M, Mostaed E, Mostaed A, Beanland R, Mantovani D, Vedani M. Fabrication, mechanical properties and in vitro degradation behavior of newly developed Zn Ag alloys for degradable implant applications. Mater Sci Eng C. 2017;77:1170–81.
89. Wang Y, Liu G, Wei Y, Qiao Y. Effects of magnesium-calcium alloys with different calcium content on their mechanical properties. IOP Conf Ser Mater Sci Eng. 2020;735(1).
90. Jia HM, Feng XH, Yang YS. Microstructure of directionally solidified Mg-Zn alloy with different growth rates. Mater Sci Forum. 2015;816:411–7.
91. Bakhsheshi-Rad HR, Hamzah E, Fereidouni-Lotfabadi A, Daroonparvar M, Yajid MAM, Mezbahul-Islam M, et al. Microstructure and bio-corrosion behavior of Mg-Zn and Mg-Zn-Ca alloys for

biomedical applications. Mater Corros. 2014;65(12):1178–87.

92. Zivić F, Grujović N, Manivasagam G, Richard C, Landoulsi J, Petrović V. The potential of magnesium alloys as bioabsorbable / biodegradable implants for biomedical applications. Tribol Ind. 2014;36(1):67–73.
93. Tao JX, Zhao MC, Zhao YC, Yin DF, Liu L, Gao C, et al. Influence of graphene oxide (GO) on microstructure and biodegradation of ZK30-xGO composites prepared by selective laser melting. J Magnes Alloy. 2020;8(3):952–62.
94. Medina S, Mendoza E, Meza JM. Comportamiento microestructural de una fundición de magnesio puro con control en la temperatura de solidificación. Univ Tecnológica PereiraScientia Tech Año XXII. 2017;22(2):145–9.
95. Wang K, Dou X, Wang J, Huang Y, Gavras S, Hort N, et al. Achieving enhanced mechanical properties in Mg-Gd-Y-Zn-Mn alloy by altering dynamic recrystallization behavior via pre-ageing treatment. Mater Sci Eng A [Internet]. 2020;790(June):139635. Available from: https://doi.org/10.1016/j.msea.2020.139635.
96. Jardim PM, Solórzano G, Sande JBV. Second phase formation in melt-spun Mg-Ca-Zn alloys. Mater Sci Eng A. 2004;381(1–2):196–205.
97. Dutta S, Gupta S, Roy M. Recent Developments in Magnesium Metal-Matrix Composites for Biomedical Applications: A Review. ACS Biomater Sci Eng. 2020;17(Table 1).
98. Bazhenov V, Koltygin A, Komissarov A, Li A, Bautin V, Khasenova R, et al. Gallium-containing magnesium alloy for potential use as temporary implants in osteosynthesis. J Magnes Alloy. 2020;8(2):352–63.
99. Bowen PK, McNamara CT, Mills OP, Drelich J, Goldman J. FIB-TEM Study of Magnesium Corrosion Products after 14 Days in the Murine Artery. ACS Biomater Sci Eng. 2015;1(10):919–26.
100. Moritz N, Strandberg N, Zhao DS, Mattila R, Paracchini L, Vallittu PK, et al. Mechanical properties and in vivo performance of load-bearing fiber-reinforced composite intramedullary nails with improved torsional strength. J Mech Behav Biomed Mater. 2014;40:127–39.
101. ISO. ISO 10993-12:2012(en), Biological evaluation of medical devices — Part 12: Sample preparation and reference materials.
102. Gai X, Liu C, Wang G, Qin Y, Fan C, Liu J, et al. A novel method for evaluating the dynamic biocompatibility of degradable biomaterials based on real-time cell analysis. Regen Biomater. 2020;7(3):321–9.
103. Zhuang Y, Liu Q, Jia G, Li H, Yuan G, Yu H. A Biomimetic Zinc Alloy Scaffold Coated with Brushite for Enhanced Cranial Bone Regeneration. ACS Biomater Sci Eng. 2020.
104. Guan RG, Johnson I, Cui T, Zhao T, Zhao ZY, Li X, et al. Electrodeposition of hydroxyapatite coating on Mg-4.0Zn-1.0Ca-0.6Zr alloy and in vitro evaluation of degradation, hemolysis, and cytotoxicity. J Biomed Mater Res - Part A. 2012;100(4):999–1015. A(.
105. Cahyono NA, Sulistyani LD, Santosa AS, Latief BS. Analysis of the mechanical properties of magnesium equal-channel angular pressing of a plate on mandibular fracture through bending and

ductility tests in physiological fluids of Dulbecco's Modified Eagle Medium. J Phys Conf Ser. 2018;1073(6).

106. Mayama T, Tane M, Tadano Y. Crystal plasticity analysis of anisotropic deformation behavior of porous magnesium with oriented pores. J Phys Conf Ser. 2018;1063(1).
107. Fattah-alhosseini A, Chaharmahali R, Babaei K. Effect of particles addition to solution of plasma electrolytic oxidation (PEO) on the properties of PEO coatings formed on magnesium and its alloys: A review. J Magnes Alloy [Internet]. 2020;8(3):799–818. Available from: https://doi.org/10.1016/j.jma.2020.05.001.
108. Mguni LL, Mukenga M, Muzenda E, Jalama K, Meijboom R. Expanding the synthesis of Stöber spheres: Towards the synthesis of nano-magnesium oxide and nano-zinc oxide. J Sol-Gel Sci Technol. 2013;66(1):91–9.
109. Kanti De A, Mukhopadhyay A, Sen S, Puri IK. Numerical simulation of early stages of oxide formation in molten aluminium-magnesium alloys in a reverberatory furnace. Model Simul Mater Sci Eng. 2004;12(3):389–405.
110. Gulbransen EA. The Oxidation and Evaporation of Magnesium at Temperatures from 400° to 500° C. Trans Electrochem Soc. 1945;87(1):589.
111. Ren F, Xin R, Ge X, Leng Y. Characterization and structural analysis of zinc-substituted hydroxyapatites. Acta Biomater [Internet]. 2009;5(8):3141–9. Available from: http://dx.doi.org/10.1016/j.actbio.2009.04.014.
112. LeGeros RZLGJ. Dense hydroxyapatite. An introduction to bioceramics. World Sci. 1993;1.
113. Tripathy NK, Patel PN. AP. Preparation, IR, and lattice constant measurements of mixed (Ca + Cu + Zn) hydroxylapatites. J Solid State Chem. 1989;80(1):1–5.
114. Paul S, Ramasamy P, Das M, Mandal D, Renk O, Calin M, et al. New Mg-Ca-Zn amorphous alloys: Biocompatibility, wettability and mechanical properties. Materialia. 2020;12(February).
115. Fazel Anvari-Yazdi A, Tahermanesh K, Hadavi SMM, Talaei-Khozani T, Razmkhah M, Abed SM, et al. Cytotoxicity assessment of adipose-derived mesenchymal stem cells on synthesized biodegradable Mg-Zn-Ca alloys. Mater Sci Eng C. 2016 Dec 1;69:584–97.
116. Zhang C, Lin J, Nguyen NYT, Guo Y, Xu C, Seo C, et al. Antimicrobial Bioresorbable Mg-Zn-Ca Alloy for Bone Repair in a Comparison Study with Mg-Zn-Sr Alloy and Pure Mg. ACS Biomater Sci Eng. 2020;6(1):517–38.
117. Zhang H, Zhao C, Wen J, Li X, Fu L. Synthesis and structural characteristics of magnesium and zinc doped hydroxyapatite whiskers. Ceram - Silikaty. 2017;61(3):244–9.
118. Rahim MI, Babbar A, Lienenklaus S, Pils MC, Rohde M. Degradable magnesium implant-associated infections by bacterial biofilms induce robust localized and systemic inflammatory reactions in a mouse model. Biomed Mater. 2017;12(5).
119. Willumeit-Römer R. The Interface Between Degradable Mg and Tissue. Jom. 2019;71(4):1447–55.

120. Cicha I, Singh R, Garlichs CD, Alexiou C. Nano-biomaterials for cardiovascular applications: Clinical perspective. J Control Release [Internet]. 2016;229:23–36. Available from: http://dx.doi.org/10.1016/j.jconrel.2016.03.015.
121. Dasgupta S, Banerjee SS, Bandyopadhyay A, Bose S. Zn- and Mg-doped hydroxyapatite nanoparticles for controlled release of protein. Langmuir. 2010;26(7):4958–64.
122. Nassif N, Ghayad I. Corrosion protection and surface treatment of magnesium alloys used for orthopedic applications. Adv Mater Sci Eng. 2013;2013.
123. Rueda LM, Nieves C, Hernández Barrios CA, Coy AE, Viejo F. Design of TEOS-GPTMS sol-gel coatings on rare-earth magnesium alloys employed in the manufacture of orthopaedic implants. J Phys Conf Ser. 2016;687(1).
124. Search H, Journals C, Contact A, Iopscience M, Address IP, Wang AM, et al. Study on constitutive model and dynamic recrystallization softening behavior of AZ80A magnesium alloy. 2017.
125. Gummow RJ, He Y. Morphology and Preferred Orientation of Pulse Electrodeposited Magnesium. J Electrochem Soc. 2010;157(4):E45.
126. Park M, Kim K. Basal texture formation behavior of M1 magnesium alloy during high-temperature compression deformation. J Phys Conf Ser. 2019;1270(1).
127. Priyanto TH, Insani A, Muslih R, Bharoto. Texture Analysis on the AZ31 Magnesium Alloy Using Neutron Diffraction Method. J Phys Conf Ser. 2020;1436(1).
128. Yan J, Qin Z, Yan K. Mechanical properties and microstructure evolution of Mg-6 wt % Zn alloy during equal-channel angular pressing. Metals (Basel). 2018;8(10).
129. Wang Y, Liu G, Wei Y, Qiao Y. Effects of magnesium-calcium alloys with different calcium content on their mechanical properties. IOP Conf Ser Mater Sci Eng. 2020;735(1).
130. Gu XN, Li N, Zhou WR, Zheng YF, Zhao X, Cai QZ, et al. Corrosion resistance and surface biocompatibility of a microarc oxidation coating on a Mg-Ca alloy. Acta Biomater. 2011;7(4):1880–9.
131. Tong X, Wu G, Zhang L, Wang Y, Liu W, Ding W. Microstructure and mechanical properties of repair welds of low-pressure sand-cast Mg–Y–RE–Zr alloy by tungsten inert gas welding. J Magnes Alloy [Internet]. 2020;(xxxx). Available from: https://doi.org/10.1016/j.jma.2020.07.009.
132. Yao X, Tang J, Zhou Y, Atrens A, Dargusch MS, Wiese B, et al. Surface modification of biomedical Mg-Ca and Mg-Zn-Ca alloys using selective laser melting: Corrosion behaviour, microhardness and biocompatibility. J Magnes Alloy [Internet]. 2020;(xxxx). Available from: https://doi.org/10.1016/j.jma.2020.08.011.
133. Chen J, Feng J, Yan L, Li H, Xiong C, Ma S. In situ growth process of Mg–Fe layered double hydroxide conversion film on MgCa alloy. J Magnes Alloy [Internet]. 2020;(xxxx). Available from: https://doi.org/10.1016/j.jma.2020.05.019.
134. Milkoreit, et al. 2018. Ac ce pte d M us pt. Geophys Res Lett. 2017;in press:0–31.
135. Krishnan K. Effect of microstructures and textures on the anisotropy of mechanical properties of AZ31 magnesium alloy sheets subjected to high strain rate rolling. J Phys D Appl Phys. 2019;in

press:0–31.

136. Mayama T, Tane M, Tadano Y. Crystal plasticity analysis of anisotropic deformation behavior of porous magnesium with oriented pores. J Phys Conf Ser. 2018;1063(1).
137. Lee J, Lee Y-S, Lee M-G, Kim D. Constitutive modelling of magnesium alloy sheets under strain path changes. J Phys Conf Ser. 2016;734:032135.
138. Sułkowski B, Janoska M, Boczkal G, Chulist R, Mroczkowski M, Pałka P. The effect of severe plastic deformation on the Mg properties after CEC deformation. J Magnes Alloy. 2020;8(3):761–8.
139. Atrens A, Liu M, Zainal Abidin NI. Corrosion mechanism applicable to biodegradable magnesium implants. Mater Sci Eng B Solid-State Mater Adv Technol. 2011;176(20):1609–36.
140. An L, Ma Y, Sun L, Wang Z, Wang S. Investigation of mutual effects among additives in electrolyte for plasma electrolytic oxidation on magnesium alloys. J Magnes Alloy. 2020;8(2):523–36.
141. Cesarz-Andraczke K, Nowosielski R. Surface Structure and Corrosion Behavior of Mg 68 – x Zn 28 + x Ca 4 (x = 0.4) Bulk Metallic Glasses after Immersion in Ringer's Solution. J Mater Eng Perform [Internet]. 2019;28(4):2365–77. Available from: https://doi.org/10.1007/s11665-019-04001-6.
142. Langelier B, Wang X, Esmaeili S. Evolution of precipitation during non-isothermal ageing of an Mg-Ca-Zn alloy with high Ca content. Mater Sci Eng A [Internet]. 2012;538:246–51. Available from: http://dx.doi.org/10.1016/j.msea.2012.01.038.
143. Wang X, Du W, Wang Z, Liu K, Li S. Stable icosahedral phase in Mg44Zn44Gd12 alloy. J Rare Earths [Internet]. 2012;30(5):503–6. Available from: http://dx.doi.org/10.1016/S1002-0721(12)60080-5.
144. Li DJ, Zeng XQ, Dong J, Zhai CQ, Ding WJ. Microstructure evolution of Mg-10Gd-3Y-1.2Zn-0.4Zr alloy during heat-treatment at 773 K. J Alloys Compd. 2009;468(1–2):164–9.
145. Damodaran VB, Murthy SN. Bio-inspired strategies for designing antifouling biomaterials. Biomater Res [Internet]. 2016;20(1):1–11. Available from: http://dx.doi.org/10.1186/s40824-016-0064-4.
146. Li X, Filek R, Zhu X, Gao H, Qiao L, Liu H, et al. Bio-modulation of scaring Glaucoma Filtration Surgery using a novel application of coated magnesium. J Magnes Alloy [Internet]. 2020;(xxxx). Available from: https://doi.org/10.1016/j.jma.2020.02.025.
147. Gungor A, Incesu A. Effects of alloying elements and thermomechanical process on the mechanical and corrosion properties of biodegradable Mg alloys. J Magnes Alloy [Internet]. 2020;(xxxx). Available from: https://doi.org/10.1016/j.jma.2020.09.009.
148. Rahman M, Li Y, Wen C. HA coating on Mg alloys for biomedical applications: A review. J Magnes Alloy [Internet]. 2020;8(3):929–43. Available from: https://doi.org/10.1016/j.jma.2020.05.003.
149. Chaharmahali R, Fattah-alhosseini A, Babaei K. Surface characterization and corrosion behavior of calcium phosphate (Ca-P) base composite layer on Mg and its alloys using plasma electrolytic oxidation (PEO): A review. J Magnes Alloy [Internet]. 2020;(xxxx). Available from: https://doi.org/10.1016/j.jma.2020.07.004.
150. Yang H, Qu X, Lin W, Chen D, Zhu D, Dai K, et al. Enhanced Osseointegration of Zn-Mg Composites by Tuning the Release of Zn Ions with Sacrificial Mg-Rich Anode Design. ACS Biomater Sci Eng.

2019;5(2):453–67.

151. Yang H, Jia B, Zhang Z, Qu X, Li G, Lin W, et al. Alloying design of biodegradable zinc as promising bone implants for load-bearing applications. Nat Commun [Internet]. 2020;11(1):1–16. Available from: http://dx.doi.org/10.1038/s41467-019-14153-7.
152. Tie D, Guan R, Liu H, Cipriano A, Liu Y, Wang Q, et al. An in vivo study on the metabolism and osteogenic activity of bioabsorbable Mg-1Sr alloy. Acta Biomater [Internet]. 2016;29:455–67. Available from: http://dx.doi.org/10.1016/j.actbio.2015.11.014.
153. Lu Y, Wang H, Liu J, Ouyang L, Zhu M. Destabilizing the dehydriding thermodynamics of MgH2 by reversible intermetallics formation in Mg – Ag – Zn ternary alloys. J Power Sources [Internet]. 2018;396(April):796–802. Available from: https://doi.org/10.1016/j.jpowsour.2018.06.060.
154. Wasiur-Rahman S, Medraj M. Critical assessment and thermodynamic modeling of the binary Mg-Zn, Ca-Zn and ternary Mg-Ca-Zn systems. Intermetallics [Internet]. 2009;17(10):847–64. Available from: http://dx.doi.org/10.1016/j.intermet.2009.03.014.
155. Liao H, Kim J, Lee T, Song J, Peng J, Jiang B, et al. Effect of heat treatment on LPSO morphology and mechanical properties of Mg–Zn–Y–Gd alloys. J Magnes Alloy [Internet]. 2020;(xxxx):4–11. Available from: https://doi.org/10.1016/j.jma.2020.06.009.

Figures

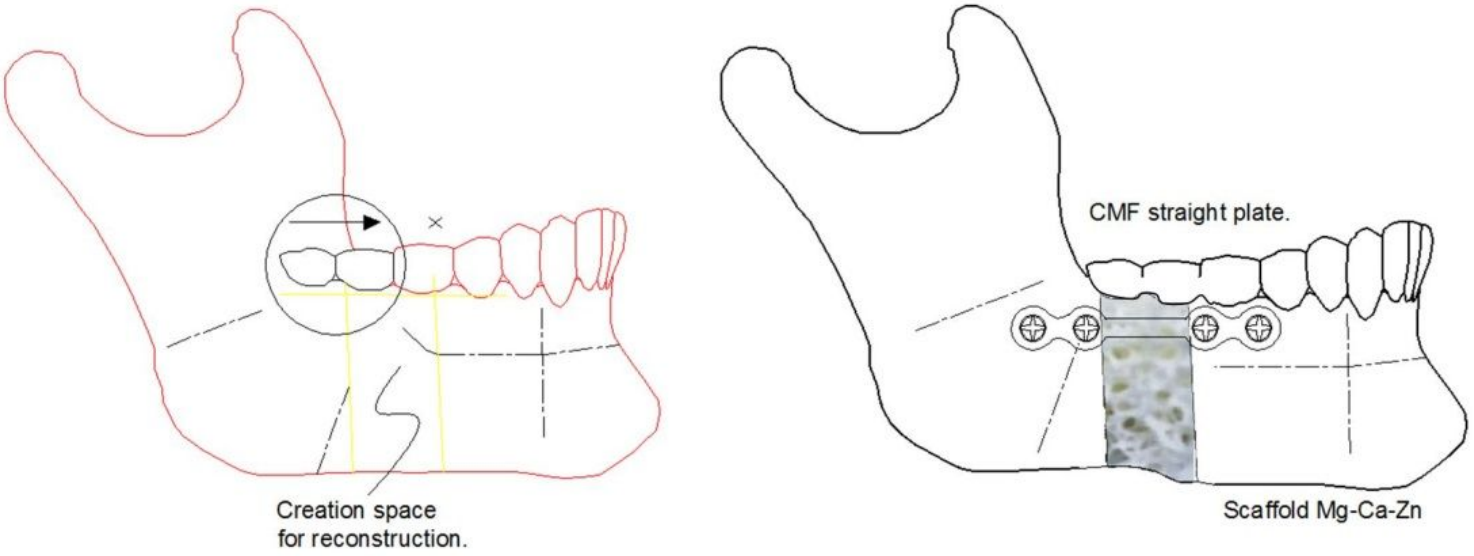

Figure 1

Lengthening of the mandibular body.

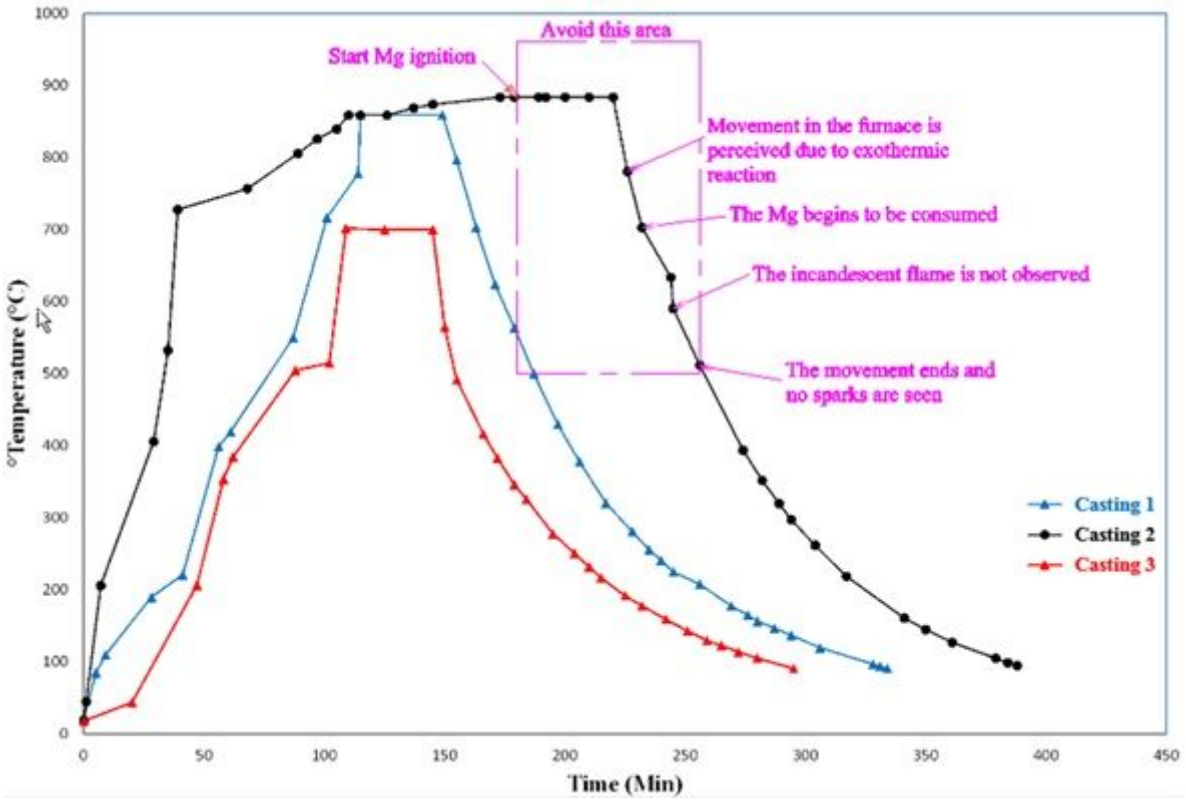

Figure 2

Casting 3; Heating ramp 6.42 ° C min^{-1}, homogenization 36 min - 700 ° C, cooling ramp 4.06 ° C min^{-1}.

Figure 3

Mg - 25 wt% Ca + 5 wt% Zn

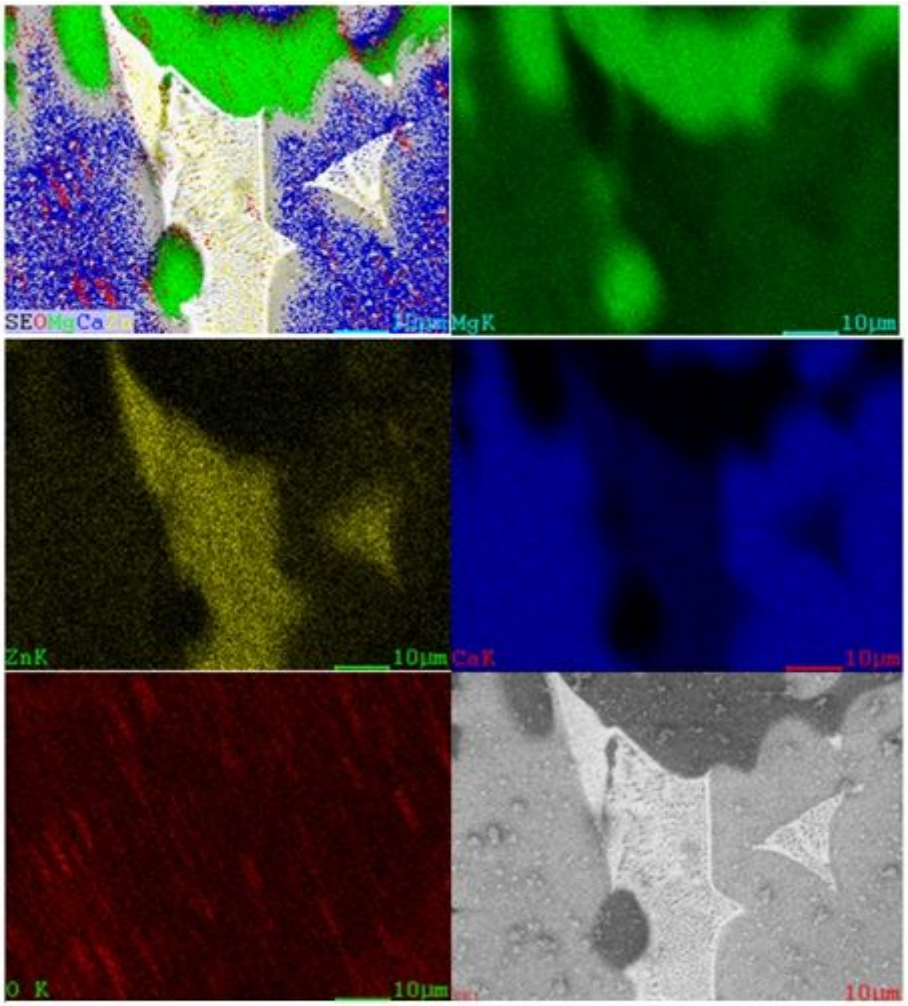

Figure 4

Element mapping by SEM-EDS (O, Mg, Ca, Zn) distribution of second phase particles.

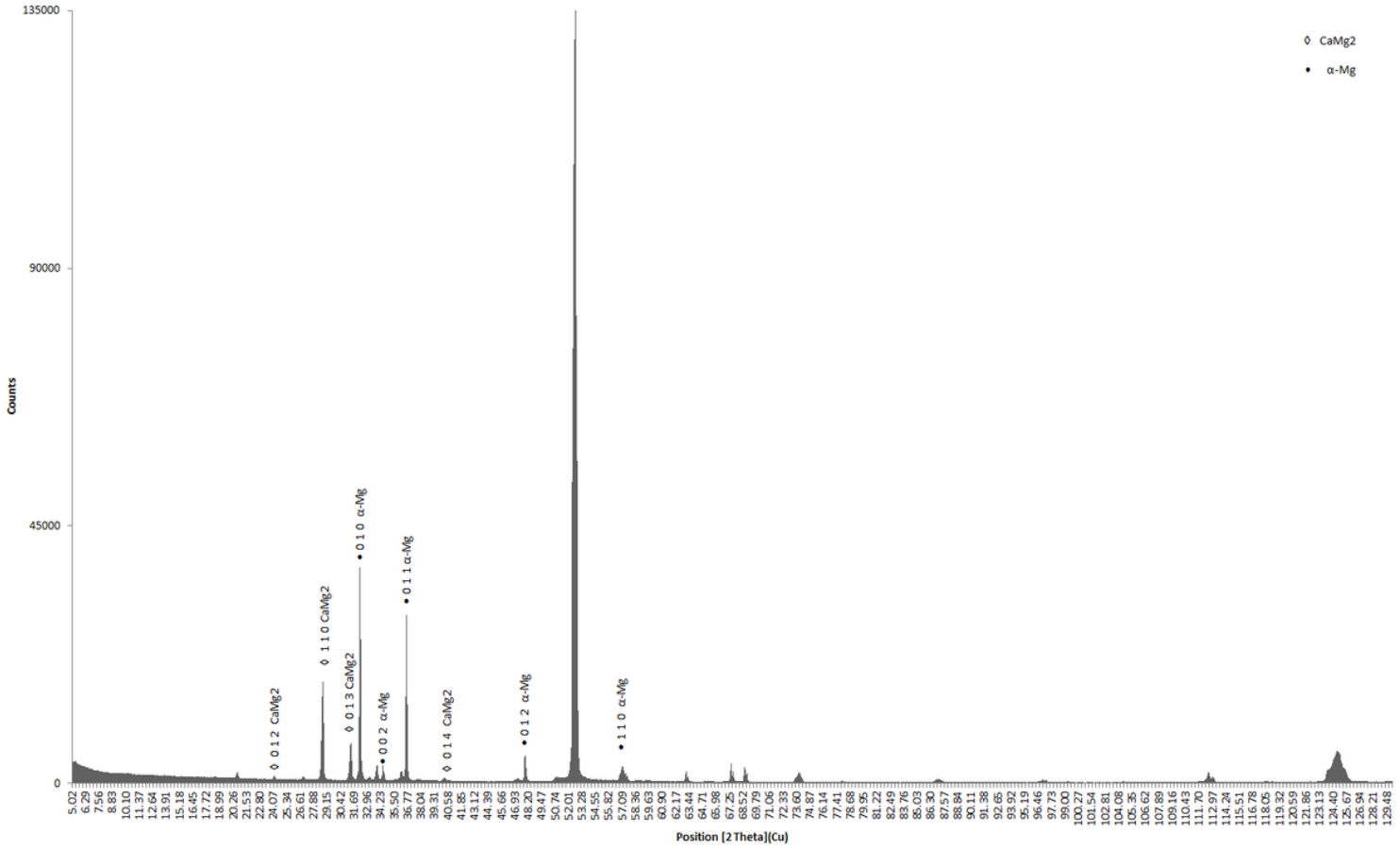

Figure 5

Patrón de difracción Mg – 25 wt% Ca + 5 wt% Zn.

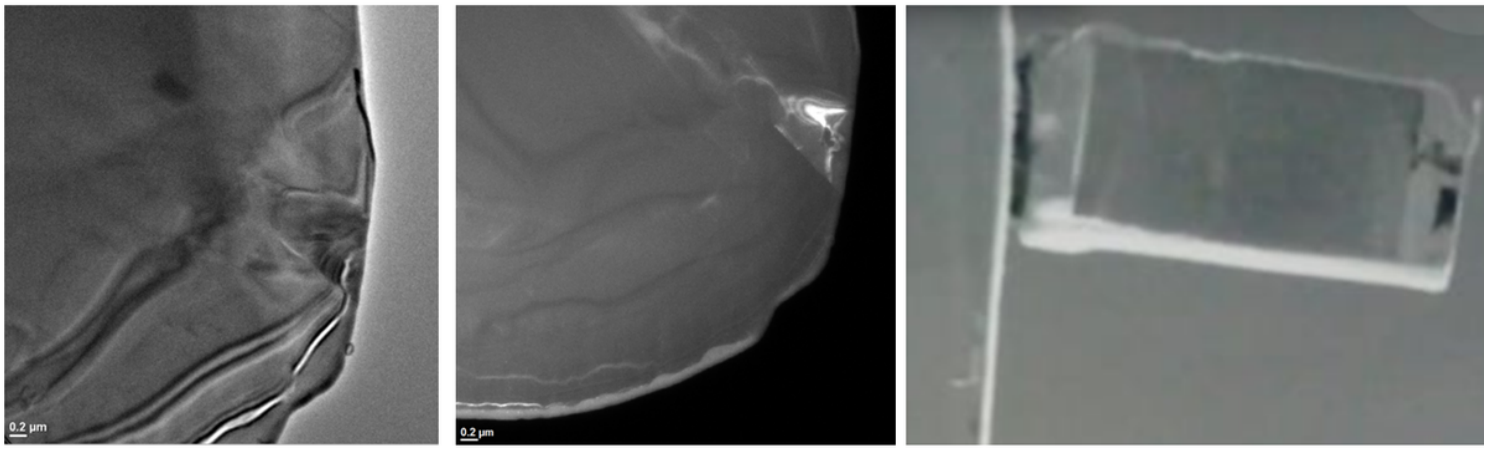

Figure 6

Bright field, dark field, and preparation of lamella by Focus ion Beam (FIB).

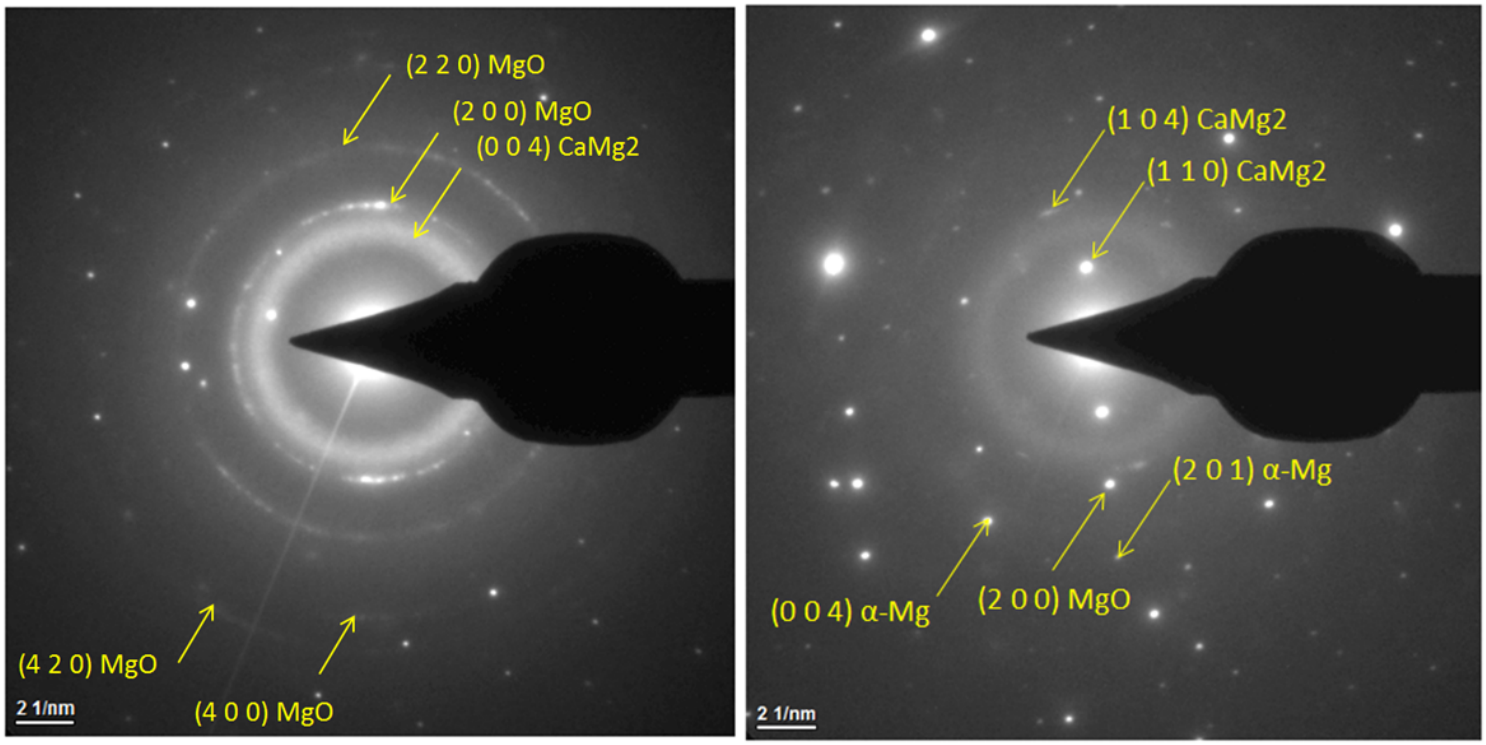

Figure 7

Diffraction patterns and identification to the α-Mg, CaMg2 & MgO phases identified by XRD, referenced to diffraction charts of the International center for diffraction data (ICDD)

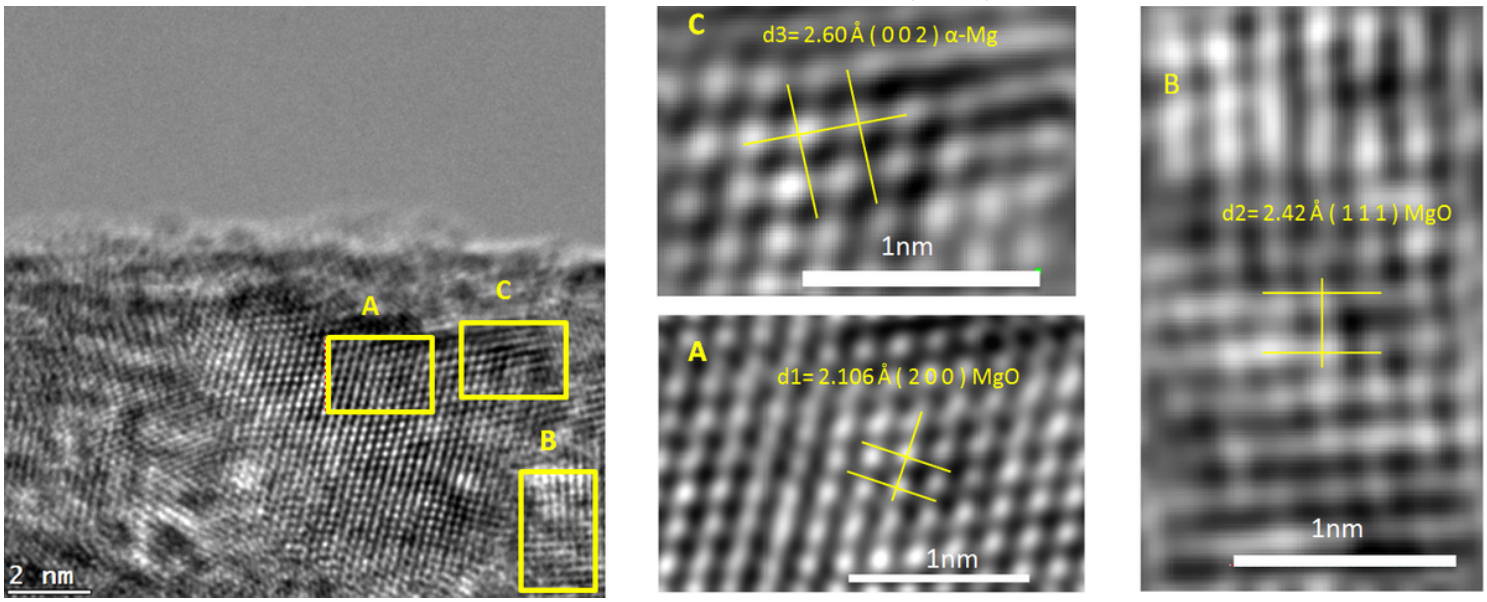

Figure 8

Plane identification with respect to interplanar space measurement on Mg – 25wt% Ca – 5wt% Zn, HRTEM images taken from sites marked A, B & C. Its relationship to MgO & α-Mg is observed.

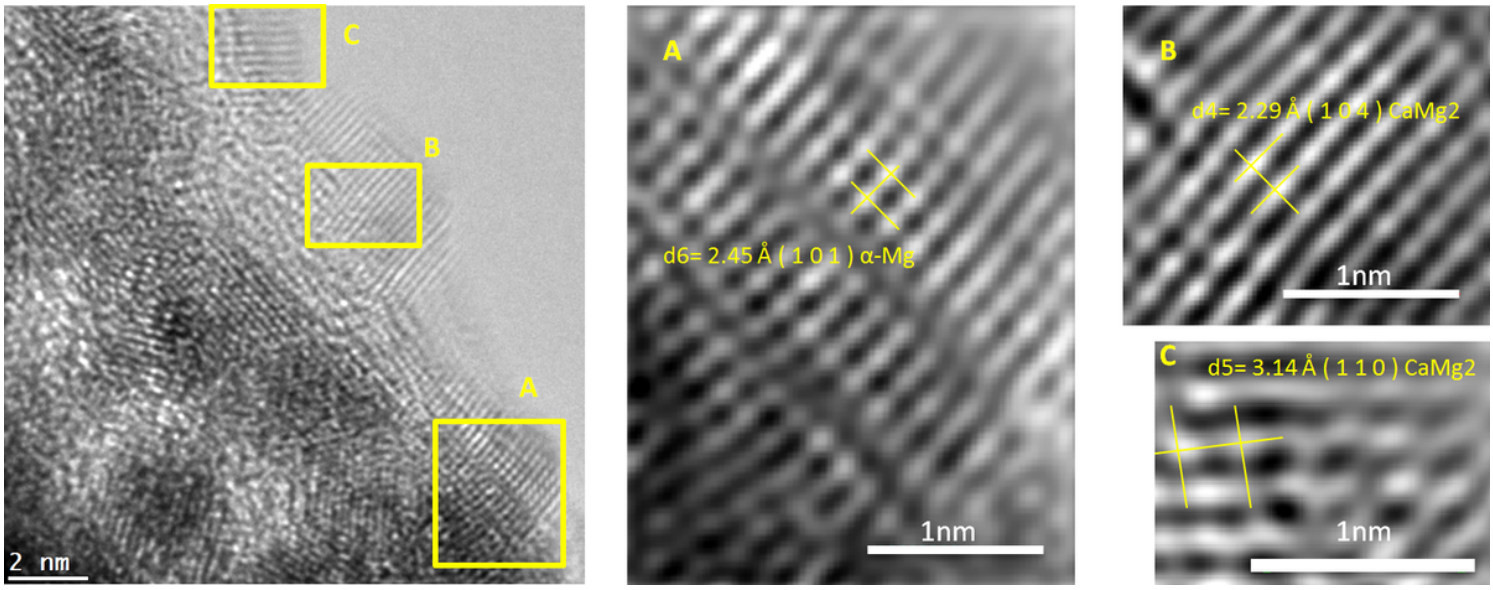

Figure 9

Plane identification with respect to interplanar space measurement on Mg – 25wt% Ca – 5wt% Zn, HRTEM images taken from sites marked A, B & C. Its relationship between α-Mg & CaMg2 is observed.

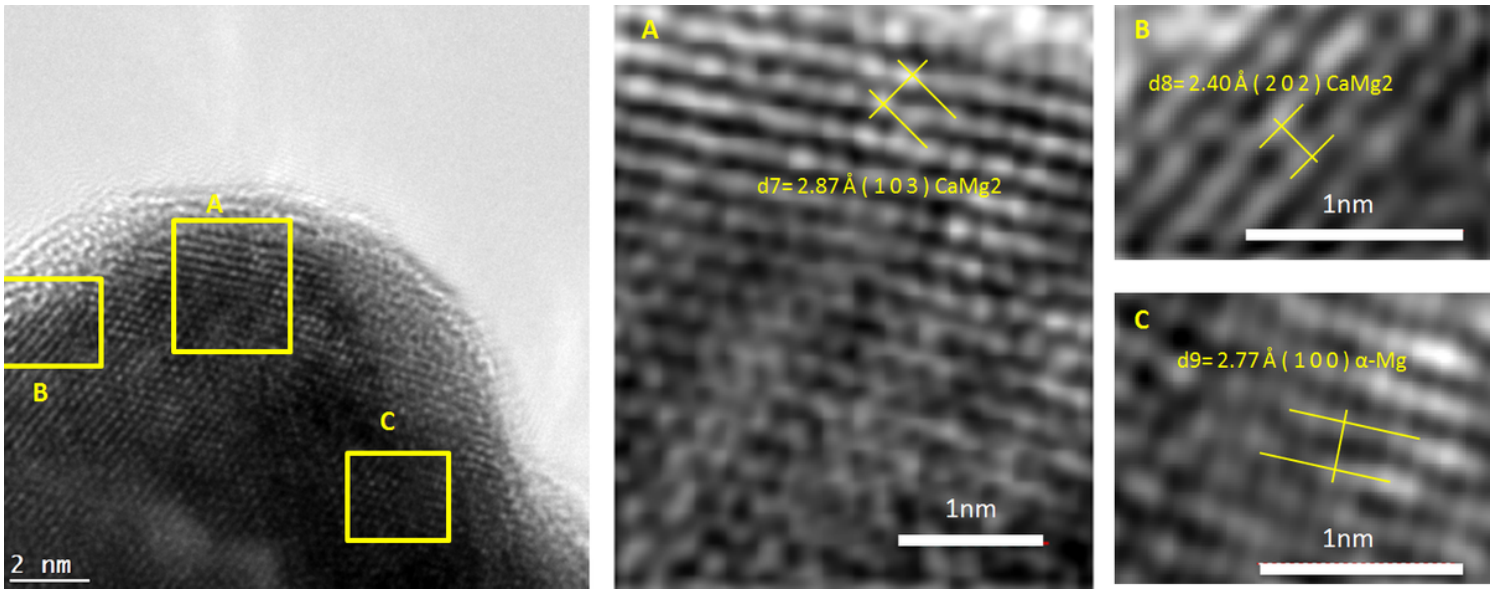

Figure 10

Plane identification with respect to interplanar space measurement on Mg – 25wt% Ca – 5wt% Zn, HRTEM images taken from sites marked A, B & C. Its relationship between CaMg2 & α-Mg is observed.

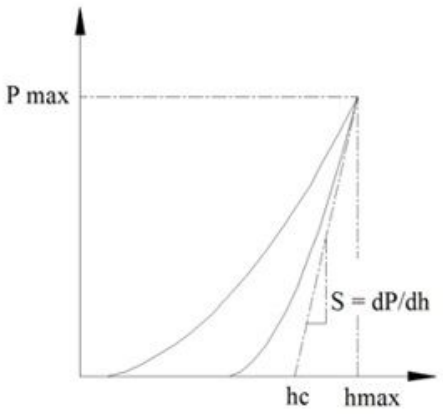

	Longitudinal (SD)	Transversal (SD)
Elastic Modulus, GPa	74.21 (2.3)	66.21 (2.5)
Hardness, HV	278.94 (0.061)	264.35 (0.082)
Pmax, mN	20.46	20.46
hmax, nm	531.18	481.75
S, mN/nm	0.2379	0.2137
hc, nm	418.62	410.96

Figure 11

Load-displacement curve, hmax: maximum penetration, S: tangent discharge curve (stiffness), hc: contact depth. Elastic moduli and hardness for Mg - 25 wt% Ca + 5 wt% Zn.

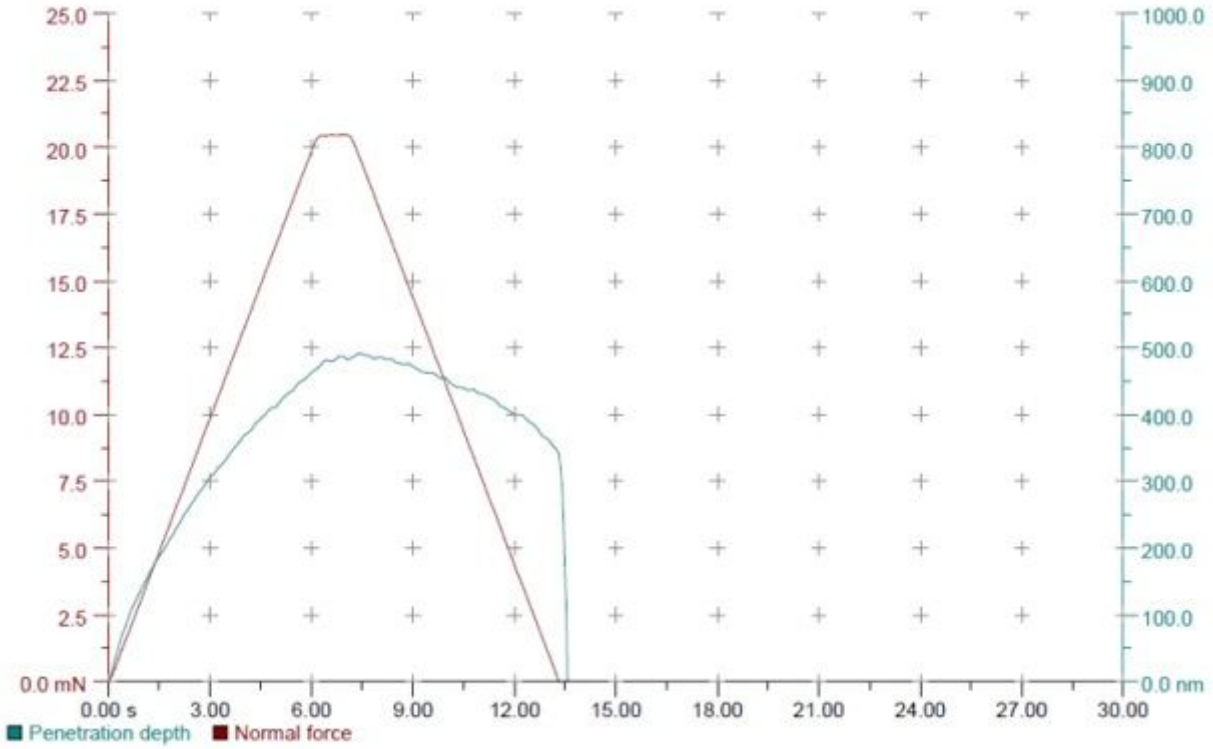

Figure 12

Force-Penetration depth.

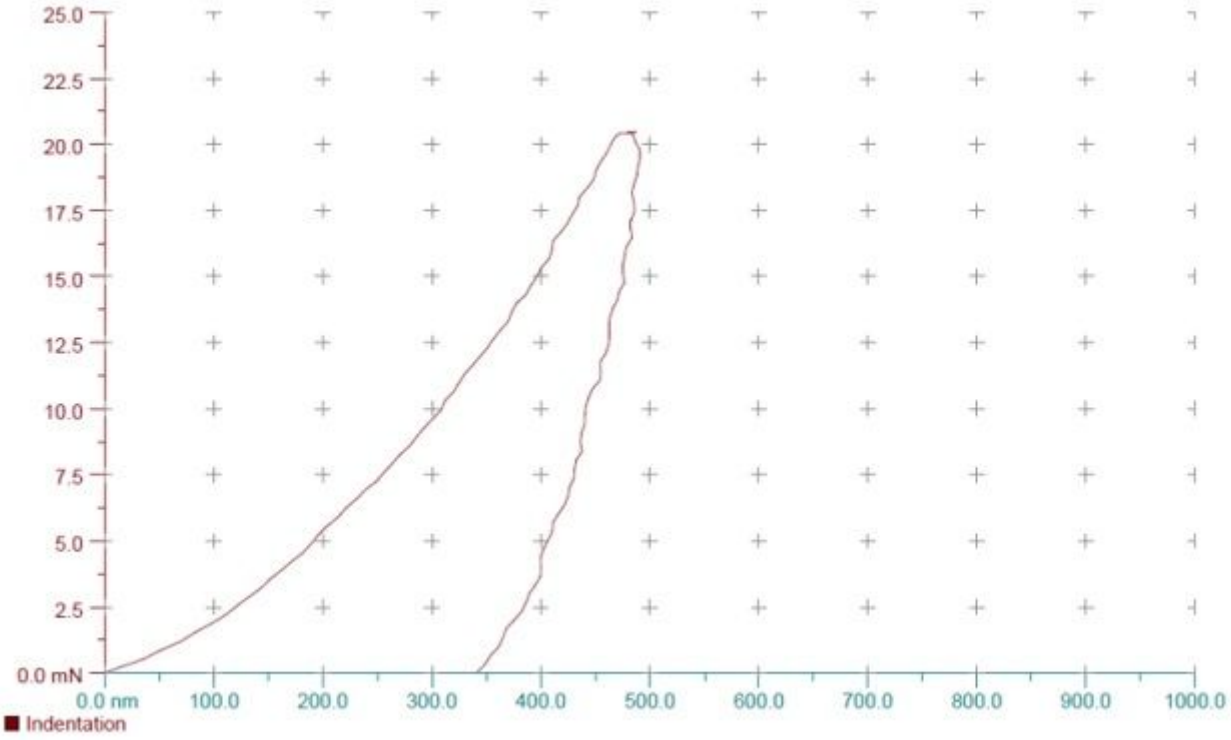

Figure 13

Force-Indentation

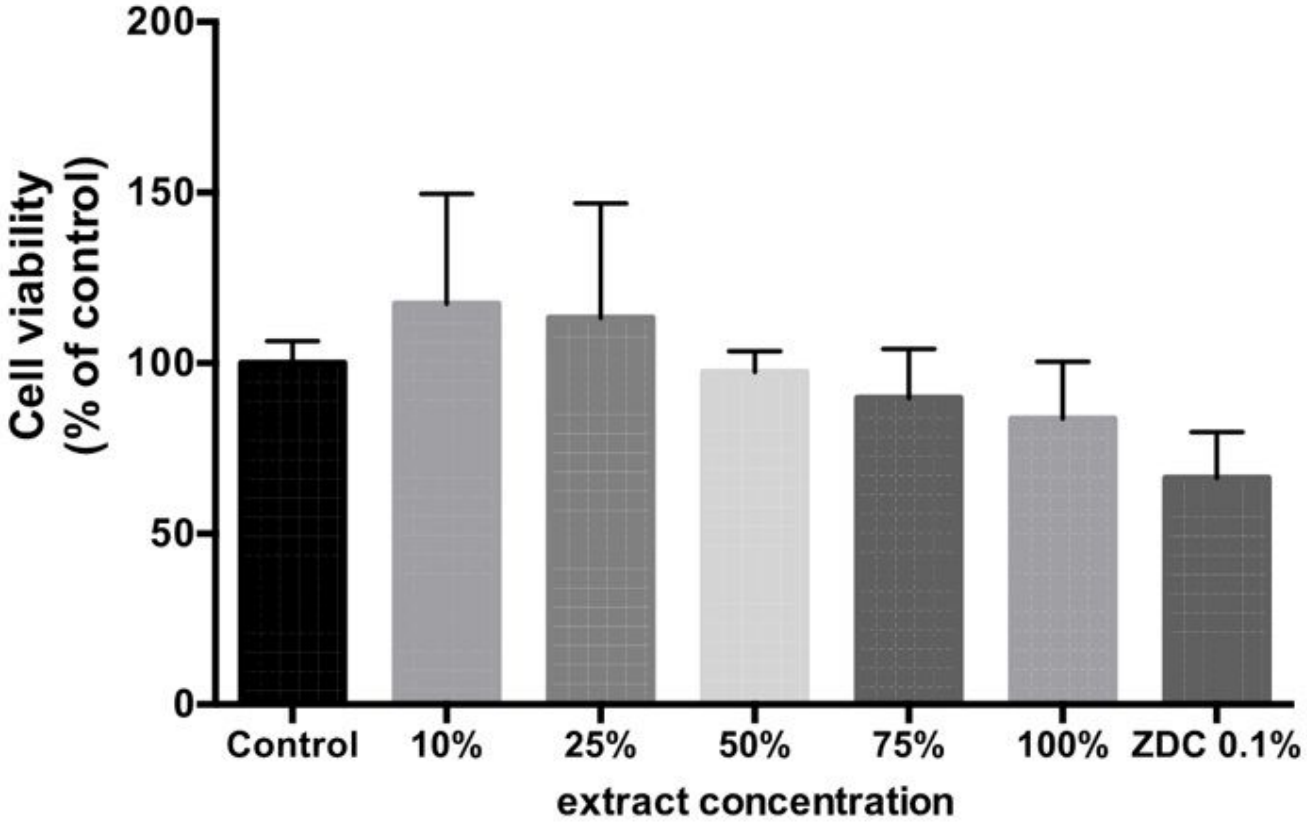

Figure 14

The effect of Mg – 25 wt% Ca + 5 wt% Zn extracts in the viability of L-929 murine fibroblasts. The graph represents results obtained after 48 hours incubation with nonserial dilutions of Mg – 25 wt% Ca + 5 wt% Zn extracts as assayed by the neutral red uptake assay (n = 4). Data are expressed as media ± standard deviation in percentage relative to the control (cell culture medium). Note that there are not significant differences between treatments, P>0.05.

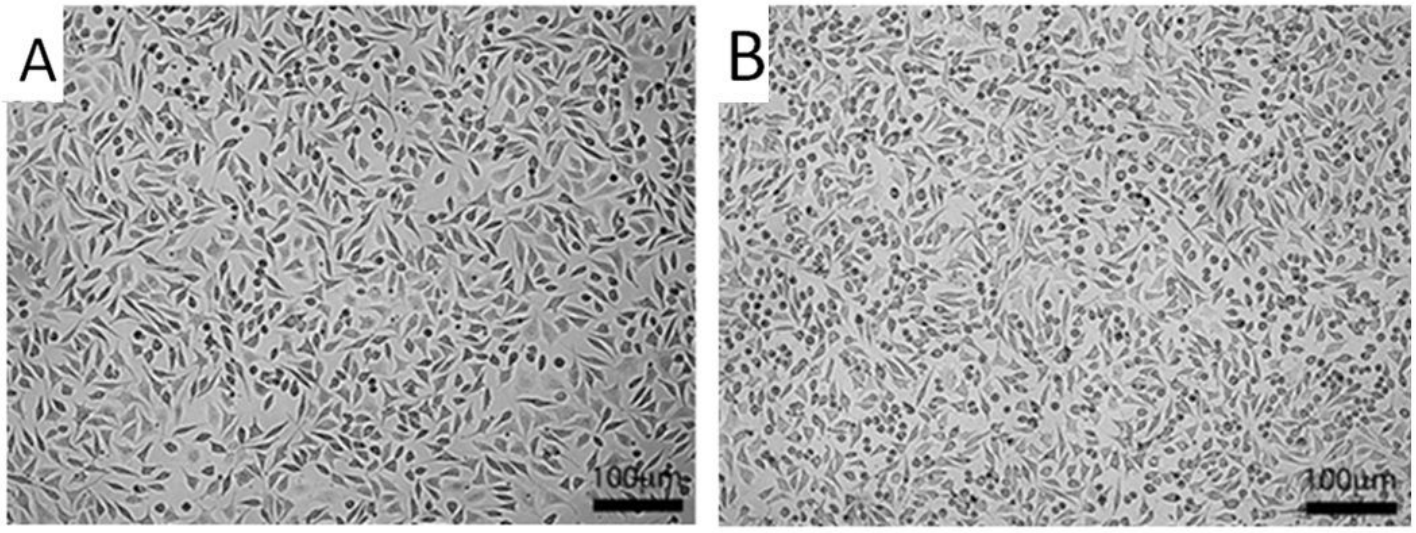

Figure 15

Representative micrographs of non-exposed cells (negative control; A) And B cells exposed to the original extracts of Mg – 25 wt% Ca + 5 wt% Zn after two days of same culture conditions. Magnification 10x, scale bar 100 µm.

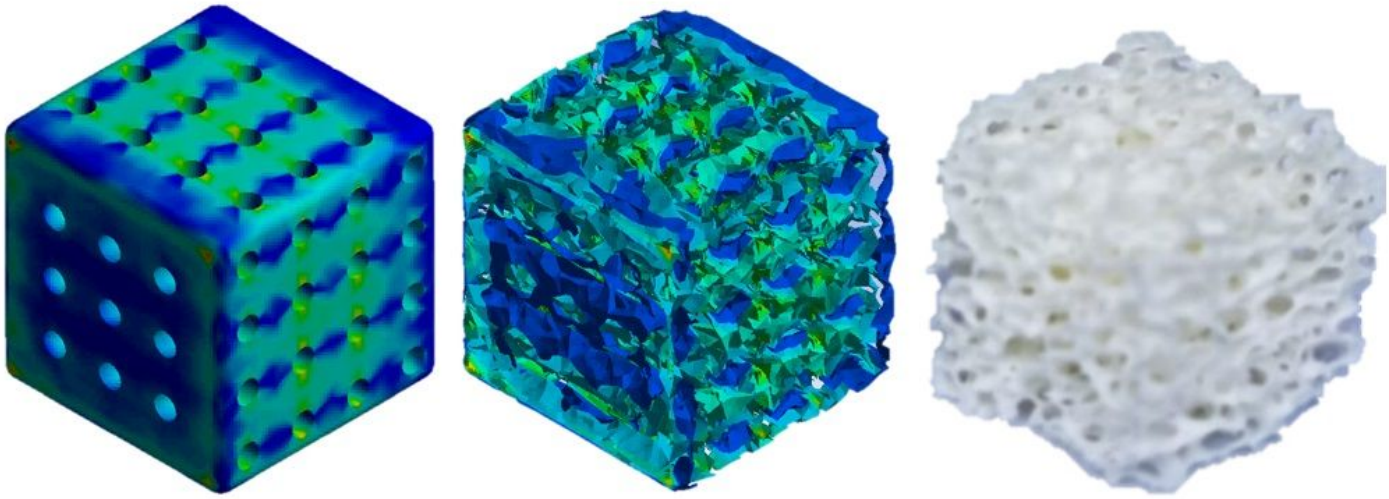

Figure 16

Scaffold load progression and comparison to DBM.